Journal of Thermal Science Vol.30, No.3 (2021) 782−806

https://doi.org/10.1007/s11630-020-1381-4 **Article ID: 1003-2169(2021)03-0782-25**

A Critical Review of Real Gas Effects on the Regenerative Refrigerators

CAO Qiang[1,2], LUAN Mingkai[1], LI Peng[1], WEI Li[3], WU Yan[1*]

1. Institute of Refrigeration and Cryogenics, School of Mechanical Engineering, Tongji University, Shanghai 201804, China
2. Shanghai Key Laboratory of Vehicle Aerodynamics and Vehicle Thermal Management Systems, Tongji University, Shanghai 201804, China
3. Department of Electrical Engineering, School of Electronics and Information Engineering, Tongji University, Shanghai 201804, China

Abstract: The regenerative refrigeration is an important reverse work-heat conversion cycle with a theoretical coefficient of performance (COP) identical to the Carnot efficiency. Practical regenerative refrigerators are capable of working down to 4 K and largely fulfill the refrigeration requirement of modern technologies in many fields, especially for space applications. However, the enthalpy flow associated with the pressure dependence, abbreviated as pressure-induced enthalpy flow, brought about by real gas effects degrades the theoretical COP of the refrigerator to below about 30% of the Carnot efficiency at the temperatures of below the critical point. This paper reviews the long history of exploring the real gas effects which dates back to the 1970s and continues to now. Important explorations of uncovering the loss mechanism and reducing such losses are summarized. The theories that are in accordance with experimental results and simulation results are expounded. We further carry out analyses on the expansion components, including the pulse tube and the clearance gap. Several inferences are made in order to explore the long-lasting puzzles about real gas effects. It is emphasized that the underlying cause of the loss in the regenerator is an indirect effect of the real gas properties. Further study about carrying out a direct verification of the theory is proposed.

Keywords: real gas effects, regenerative refrigerators, loss mechanism, reduction methods

1. Introduction

The refrigerator is one kind of reverse work-heat conversion machine that removes heat from a low-temperature reservoir. Regenerative refrigerators are widely used for cryogenic applications because of the advantages of high reliability [1], compactness [1], high efficiency [2] and low temperature oscillation [3], which make them very appealing for small-scale and mid-scale applications [4], especially for space applications [5].

In principle, the regenerative refrigerator is possible to achieve a low temperature even close to absolute zero with the highest possible efficiency, i.e. Carnot coefficient of performance (COP) [6]. The precondition is a set of lossless hardware as well as working with an ideal gas. However, there will be some losses if working with a real gas because of real gas effects. The specific enthalpy of an ideal gas is only a function of temperature,

Received: Jul 20, 2020 Article type: Invited Review Corresponding author: WU Yan E-mail: yan.wu@tongji.edu.cn

Nomenclature

AC	alternative-current flow
COP	coefficient of performance
c_p	specific heat capacity/J·kg^{-1}·K^{-1}
DC	direct-current flow
$\langle \dot{H}_p \rangle$	time-averaged pressure-induced enthalpy flow/W
$\langle \dot{H}_T \rangle$	time-averaged heat-associated enthalpy flow/W
k_T	coefficient between $\langle \dot{H}_T \rangle$ and temperature gradient
$\dot{m}$	mass flux/kg·s^{-1}
P_r	pressure ratio
PTR	pulse tube refrigerator
p	pressure/MPa
$\langle p\dot{V} \rangle$	PV power/acoustic power/W
$\langle \dot{Q} \rangle$	heat flow or refrigeration power/W
$\langle \dot{Q}_{loss} \rangle$	heat loss in the pulse tube/W
rCOP	relative Carnot COP
$\langle \dot{S} \rangle$	time-averaged entropy flow/W·K^{-1}
T	temperature/K
t	time/s
U	internal energy/W
v	specific volume/m^3·kg^{-1}
x	position/mm
Z	compressibility factor

Greek letters

β	volume expansivity/K^{-1}
ε	attenuation coefficient of heat load

Subscripts

0	mean (pressure)
c	cold end
cond	conduction
DC	direct-current flow
ex	exit flow
g	gas
gen	(entropy) generation
gross	gross (refrigeration power)
h	hot end
i	index
in	inflow
max	maximum
min	minimum
n	number of grid
net	net (refrigeration power)
prec	precooling
PT	pulse tube
R	regenerator
r	reduced
T	temperature related
tot	total amount
x	unfixed position

while that of a real gas is a function of both temperature and pressure. The real gas effects on the regenerative refrigerator are mainly about the pressure-induced enthalpy flow, which stems from the two factors of molecular volume and the molecule interaction in real gases. Actually the COP is very low when the refrigeration temperature is close to or below the critical point. It is worth a comprehensive review of both theoretical and experimental studies about real gas effects on regenerative refrigerators.

1.1 Working mechanism of regenerative refrigerators

There are two types of regenerative refrigerators according to the driving system, one is Gifford-McMahon (GM) type with valves and the other is the valveless Stirling type [7]. The former type includes the GM refrigerator and the GM-type pulse tube refrigerator (PTR), and the later type includes the Stirling refrigerator and the Stirling-type PTR.

The working mechanism of the regenerator and the phase shifter are the same for both types, but the driving system is quite different. There is a significant irreversibility in the valves of the GM type, while the ideal Stirling-type compressor is lossless, so the Stirling-type refrigerator is preferred for a theoretical analyzing. A sketch of a Stirling refrigerator and a Stirling-type PTR is shown in Fig. 1.

The Stirling refrigerator generally applies a regenerator and pistons at the hot end and cold end [7]. The piston at the hot end provides an input power in an alternating pressure-volume form (i.e. PV power). The ideal regenerator transports such a PV power over the temperature gradient from the hot end to the cold end in a process without a flow-friction loss or a loss related to limited heat transfer and limited matrix heat capacity. The heat of the gas is temporarily stored in the matrix with no temperature difference. The PV power at the cold end is recovered with a piston (or specified as

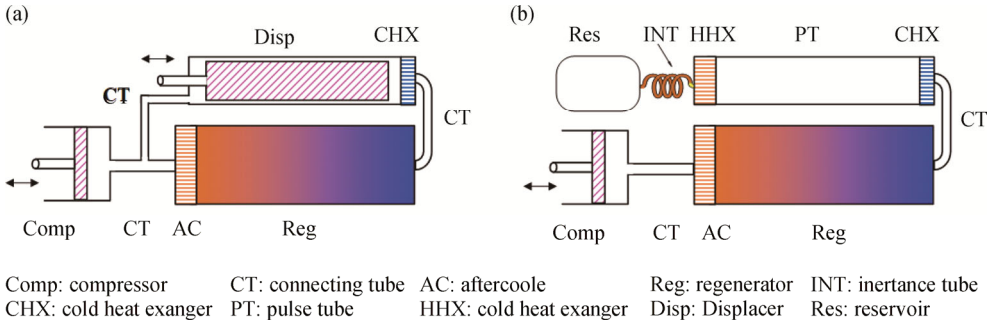

Fig. 1 Schematics of two typical regenerative refrigerators, a Stirling refrigerator (a) and a pulse tube refrigerator with an inetance tube as the phase shifter (b)

"expander"), so that a refrigeration power is generated. The PTR works without a piston at the cold end, but there is a pulse tube that transports the PV power from the cold end to the hot end through that hollow tube (pulse tube). The PV power is dissipated in the phase shifter [7] or recovered to the compressor with a mass-spring feedback mechanism [8]. Such a recovery method is able to improve the COP of the refrigerator.

1.2 Parameters related to real gas effects and corresponding losses

The model of an ideal gas means that all collisions between atoms or molecules are perfectly elastic, and the size of the molecules and the force between molecules are omitted [9].

The model of a real gas takes into account the two important factors of the molecular-occupied volume and the interaction between molecules [9]. The volume of the molecule reduces its free space and increases the collision frequency of molecules, while the force between molecules decreases the impact force, so the corresponding state parameters will change. The compressibility factor (noted as Z) and the volume expansivity (noted as β) are such typical parameters.

Fig. 2 shows the compressibility factor of three kinds of gases [10, 11], ^{4}He, ^{3}He, and H_2, versus the reduced temperature (the temperature normalized by the critical temperature) under various reduced pressures (the pressure normalized by the critical pressure). These gases behave quite similarly when those state parameters are normalized. They actually show the general thermodynamic principles of gases. The compressibility factor gradually shifts from unity when the reduced temperature is smaller than about 4. It gradually gets smaller and then it rises with an accelerating rate. Note that the compressibility factor of an ideal gas keeps unity. The volume expansivity of an ideal gas is equal to the reciprocal of the temperature, so the combined parameter $(1–T\beta)$ keeps zero at any temperature. This parameter $(1–T\beta)$ of a real gas is related to the compressibility factor [12], and it gradually shifts from zero when the reduced temperature is smaller than about 4; it gradually gets smaller and then rises, eventually up to unity, as shown in Fig. 3.

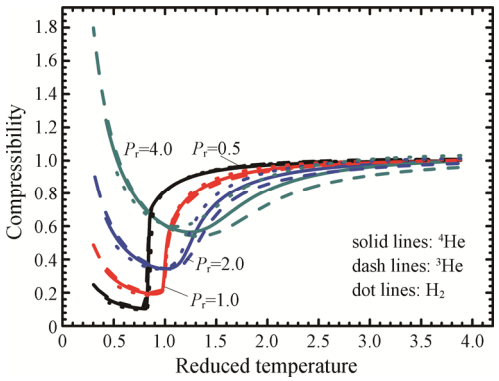

Fig. 2 Dependence of the compressibility factor on the reduced temperature for various gases. The solid, dash, and dot lines represent ^{4}He, ^{3}He, and H_2 [10, 11]. The black, red, blue, and cyan lines represent a reduced pressure of 0.5, 1.0, 2.0, and 4.0, respectively.

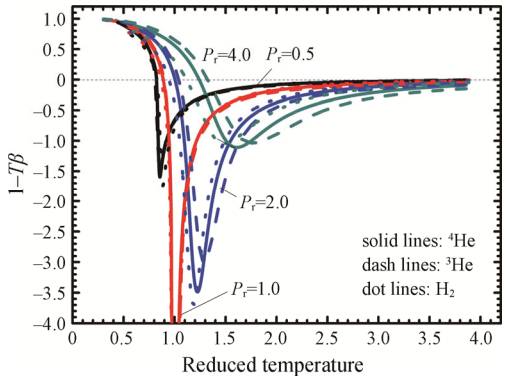

Fig. 3 Dependence of the combined parameter $(1–T\beta)$ on the reduced temperature for various gases. The solid, dash, and dot lines represent ^{4}He, ^{3}He, and H_2 [10, 11]. The black, red, blue, and cyan lines represent a reduced pressure of 0.5, 1.0, 2.0, and 4.0, respectively.

The pressure-induced enthalpy flow is proportional to the PV power with a coefficient of (1–$T\beta$) [13, 14], and the PV power of a real gas is a function of the combined parameter (ZT) [13]. So the pressure-induced enthalpy flow $\langle \dot{H}_p \rangle$ in a lossless regenerator [14] can be expressed as:

$$\langle \dot{H}_p \rangle = (1 - T\beta) ZT \left(\langle p\dot{V} \rangle_h \Big/ Z_h T_h \right) \quad (1)$$

where $\langle p\dot{V} \rangle$ is the PV power.

As will be discussed in Section 2, the pressure-induced enthalpy flow is the key points that how the real gas effects influence the energy balance in the regenerative refrigerator. Eventually, losses are generated. The losses brought about by real gas effects are generally abbreviated as real gas losses.

We have carried out calculations for several practical regenerators with the renowned numerical code of REGEG3.3 [15], which shows that the real gas loss accounts for around 70% of the total availability of the refrigerator if ^{4}He is used as the refrigeration fluid [13], as shown in Fig. 4. This loss is still larger than 60% even when the rarer isotope gas ^{3}He is charged. However, this loss is quite small (around 1%) when the temperature gets as high as 80 K or above. This is the dominant reason why the refrigeration efficiency deteriorates dramatically from about 20% (rCOP) at around 80 K to about 1% (rCOP) at around 4 K [3].

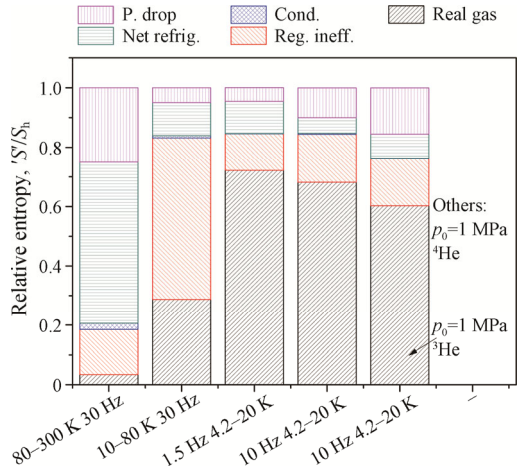

Fig. 4 Calculated loss distribution of regenerators working at various temperature ranges. The last one applies ^{3}He as the working fluid, and the others use ^{4}He. The pink, cyan, blue, red, black bars represent the relative entropy of the pressure drop, the net refrigeration power, the conduction heat loss, regenerator inefficiency ($\langle \dot{H}_T \rangle$), and real-gas loss ($\langle \dot{H}_p \rangle$), respectively.

1.3 Historical progress summary

The study of the real gas effects on the regenerative refrigerators has lasted a long history. In this review, we would like to summarize the development of the real gas effects into three periods, including: (1) Early theoretical analyses mainly in the 1980s; (2) Experimental researches since the 1990s; (3) Modern theoretical analyses since the 2000s. A brief description of these researches is listed below.

(1) Some researchers had realized the seriousness of real gas losses since the 1970s. The pressure-induced enthalpy flow and the heat-associated enthalpy flow had been pointed out, although the terms had not been clearly defined. Expressions of the refrigeration power and the COP were given. The losses were considered to be intrinsic, and thus they were impossible to decrease.

(2) Technology of regenerative refrigerators improved and 4 K was achieved with the GM-type PTR in the laboratory in the 1990s. Abundant experimental tests have been carried out since then. Temperature profiles of the regenerator and the pulse tube have been measured. Experiments about the intermediate refrigeration power, DC flow, and liquefaction have been carried out. Significant improvements of the refrigeration power or liquefaction rate have been achieved. Reduction methods of real gas losses have been pointed out.

(3) Modern theoretical analyses have been carried out based on the enthalpy theory of the oscillating flow as well as the physical properties of gases. Abundant experimental results accumulated since the 1990s provide a basis for the theoretical analyses, and many kinds of numerical software are able to provide an abundance of digital materials. A work of identifying the main factors and building a theoretical model from a macroscopic perspective has been accomplished, so the loss terms and their mechanism have been explored. Key parameters of the pressure-induced enthalpy flow and the heat-associated enthalpy flow have been clearly defined and expressed based on the gas properties. The theoretical COP and the ultimate temperature have been expressed. The reduction methods of real gas losses have been systematically explored.

We have summarized the main researches of these three periods in Table 1, which would be clear to show the progresses.

Early theoretical researches will be firstly introduced in the following section. Experimental researches and modern theoretical analyses will be reviewed in the main parts, according to various topics.

1.4 Early theoretical research about real gas effects

People started to notice the real gas effects as the regenerative refrigeration develops in history. As we know, the regenerative refrigerator was first put into application in 1874 [6], and the refrigeration temperature went down to liquid-nitrogen temperature in Philips Company in 1946 [6]. An even lower temperature of 7 K

Table 1 Main researches and feathers of the three periods about real gas effects

Period	Year	Progress on loss mechanism	Progress on loss reduction	Main methods	Achieved T_c
Early theoretical research	1970s to early 1990s	Realize real gas losses, give complex expression of heat losses, COP	None, cannot reduce "intrinsic" losses	Theoretical analyses with equations of state, simple numerical simulation	About 7 K
Experimental research	1990s up to now	Measure COP, ultimate T_c, temperature profiles of Reg (regenerator) and PT (pulse tube)	Measure intermediate refrigeration power, DC flow, liquefaction rate	Experiment	Below 4.2 K, 1.27 K
Modern theoretical analyses	2000s up to now	Determine loss terms and loss mechanism in Reg and PT, give general expression of $\langle \dot{H}_T \rangle$, $\langle \dot{H}_p \rangle$, COP	Derive theory of various methods to reduce losses in Reg and PT, possible to increase COP by times	General theoretical analyses, complex numerical simulation	Below 4.2 K

was obtained by use of multiple expansion [6]. The obstacle of obtaining the liquid-helium temperature was considered to be the thermal saturation of the regenerator matrix [6]. The classical analysis of the regenerative refrigeration was the Schmidt model [16] and the Finkelstein adiabatic model [17], which both assumed an ideal working fluid. Those models predicted the performance with fairly good accuracy. It was not considered to be necessary to take the real gas effects into account in those models.

There were researchers in the 1970s who considered the "commonly neglected" real gas behavior and pointed out that this behavior could be important [18]. Later, it was pointed out that the real gas effects reduce the refrigeration capacity of Stirling refrigerators [19].

Since the 1980s, scholars in the fields of cryogenic physics and cryogenic engineering have started to analyze this topic through numerical calculations [20–22] and analytic solutions [20, 23–25] and have revealed a number of mechanisms of the real gas effects both in the regeneration process and in the expansion process. Generally the van der Waals equation of state or improved three-parameter equations of state was used to obtain an analytical expression of the refrigeration capacity [20].

The real gas effects on the regenerators have been studied. The ideal regenerative condition was analyzed based on those equations of state, and the "excess heat" (generally regarded as the "heat-associated enthalpy flow") is obtained due to the heat imbalance in a regenerative process [24]. This inherent non-ideal regenerative "excess heat" was found to form either a low-temperature heat load or a high-temperature heat load depending on it is positive or negative.

The heat-associated enthalpy flow is the enthalpy flow associated with the imperfect heat transfer and limited matrix heat capacity in the regenerator [14], and nowadays it is determined with this equation:

$$\langle \dot{H}_T \rangle = \frac{1}{\tau} \oint \dot{m} c_{p,\mathrm{g}} T_{\mathrm{g}} \mathrm{d}t \tag{2}$$

where τ is the period time of the oscillation flow; $\dot{m}$ is the mass flow rate; $c_{p,\mathrm{g}}$ is the specific heat capacity of the gas; T_{g} is the instantaneous temperature of the gas.

The pressure difference between the period that the gas enters the expansion chamber and the period that it leaves causes a heat imbalance, which is called "missing enthalpy" (i.e. "pressure-induced enthalpy flow"), thus it brings about a heat loss at the cold end [22]. It was expressed as:

$$\langle \dot{H}_p \rangle = \oint \dot{m} \left[v - \dot{T} \left(\frac{\partial v}{\partial T} \right)_p \right] \mathrm{d}p \tag{3}$$

Note that this expression is essentially the same as the one used today.

The theoretical COP of such cycles has been expressed, and it was deduced that the COP cannot reach the Carnot COP [22, 24, 25].

However, the regenerative process of the early Stirling cycle as well as the Villemere cycle, was simplified as an isometric process [24–26] in the 1980s, and the theory on the oscillating-flow energy flow is lacking. What's more, the problem of real gas effects did not attract much attention because the refrigeration temperature was not very low (< 10 K) at that time.

When the modern thermoacoustic theory was applied to analyze the regenerator, it was found that in or during the envelope of the microcycle that each parcel run constitutes two limit lines. The pressure of each line keeps constant [27]. In addition, it was assumed that each part of the regenerator shares the same average pressure in order to analyze the internal mechanism of the regenerator [7], which has been verified through experimental measurements.

Note that the van der Waals equation of state (and improved equation) has seldom been used to calculate this issue since the late 1990s. The reasons are mainly that the calculation with equations is very complex and the accuracy is low. Due to the nonlinearity of the gas properties at the temperatures close to or below the critical point, complex equations with more than ten parameters

were often used, which sets an obstacle to analytical solutions [18]. Furthermore, the van der Waals equation of state and its improved equations have a relatively large error. For example, the density error at 10 K and 1.5 MPa reaches 49% when using the van der Waals equation of state [20]. Therefore, the real gas properties are more accurate to describe with the compressibility factor and volume expansivity. The popularity of computers makes it more convenient to invoke a physical property database through programs, as done in REGEN [15], Sage [28], and other programs [29, 30].

In this paper, we will expound the mechanism of the real gas effects on important parts of regenerative refrigerators and methods of reducing these real gas losses, mainly based on the studies in the second and third periods of history.

2. Mechanism Exploration of Real Gas Effects

Since the 1990s, a regenerator temperature profile that is far from linear at liquid-helium temperatures has been observed [31–34], as shown in Fig. 5. This phenomenon has aroused great interests in the real gas effects. A round of exploring the mechanism underneath this phenomenon began since that time.

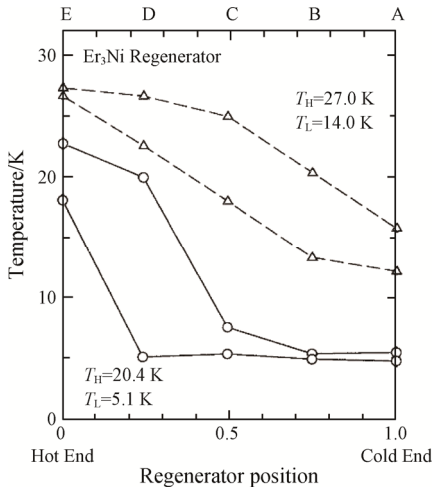

Fig. 5 Measured temperature profile of regenerator matrix for different cold-end temperature in the second-stage regenerator of a GM refrigerator [34]. The label "A–E" refers to the number of the temperature sensors (equally arranged). The dash lines refer to the cases of a hot-end temperature (T_h) of 27.0 K and a cold-end temperature (T_c) of 14.0 K. The solid lines refer to a T_h of 20.4 K and a T_c of 5.1 K.

The regenerator is the focus of most researches about real gas effects, while the real gas effects on the expansion process are also significant. The main components of the expansion process include the pulse tube in a pulse tube refrigerator and the clearance gap between the expander and the cylinder in a Stirling refrigerator or GM refrigerator. Note that the expansion space isn't influenced much by real gas effects because its temperature is largely homogeneous, and it is not discussed here. The details about the regenerator, the pulse tube, and the clearance gap are analyzed in the following.

It is reasonable to classify the researches into two classes: one is mechanism explorations of real gas effects, and the other is method studies of reducing real gas losses. The research areas related to mechanism explorations include the loss terms in the regenerator, the theoretical COP, the ultimate refrigeration temperature, and the effects on the pulse tube.

2.1 Loss terms in the regenerator

Determining the loss terms is the key point of exploring the real gas effects on the regenerator. A theoretical method that focuses on the energy balance in the regenerator for analyzing this phenomenon was proposed [35]. The first law of thermodynamics demanded that the energy flow in the regenerator ($\dot{Q}_{\text{tot}}$), which includes the heat conduction $\dot{Q}_{\text{cond}}$ and the pressure-induced enthalpy flow $\left\langle \dot{H}_p \right\rangle$, should keep constant. It was expressed as:

$$\dot{Q}_{\text{tot}} = \dot{Q}_{\text{cond}} + \left\langle \dot{H}_p \right\rangle \tag{4}$$

An assumption of a perfect thermal contact between the gas and the matrix and a large heat capacity of the matrix was made, which means that the heat-associated enthalpy flow is zero. In this case, the heat conduction was considered to be an essential role in achieving the energy balance of the regenerator [35, 36].

The temperature profile of the regenerator between a range of 300 K and 2.2 K was determined with this analysis [35]. The temperature gradient is almost zero within a large portion of the regenerator near the cold end, which is inconsistent with the measurement [31, 32], as shown in Fig. 5.

A numerical simulation of the temperature profile [29, 37] was made prior to the thermodynamic derivation discussed above [35] (shown in Fig. 6), and it is in good consistent with the experiment measurements [31, 34], shown in Fig. 5. The simulation took account of real gas properties (i.e. real gas effects were considered), limited heat transfer rate, limited heat capacity, and heat conduction, so this simulation should be closer to a practical case since not many assumptions were made. There was no conclusion about which factor shapes the temperature profile, but the temperature profile in various phases provided detailed information.

The idea of using the first law of thermodynamics [35] was used [14] to analyze the regenerator section between two heat exchangers at steady state [7]; that is to say, there is no heat exchange with external systems in this regenerator section. The explicit terms that make up the total heat flow were found to be the three terms, i.e. the heat conduction $\dot{Q}_{\mathrm{cond}}$, including that of gas, matrix and wall, the heat-associated enthalpy flow $\left\langle \dot{H}_T \right\rangle$, and the pressure-induced enthalpy flow $\left\langle \dot{H}_p \right\rangle$. The total heat flow should be kept constant and was expressed as:

$$\mathrm{d}\left(\left\langle \dot{H}_p \right\rangle + \left\langle \dot{H}_T \right\rangle + \dot{Q}_{\mathrm{cond}}\right)\Big/\mathrm{d}x = 0 \tag{5}$$

The heat-associated enthalpy flow was not assumed [14] to be zero all along the regenerator, because the calculated local temperature variation in one cycle abnormally gets as large as 8 K, as shown in Fig. 6. However, the heat-associated enthalpy flow is possible to reach the minimum value of zero at some points.

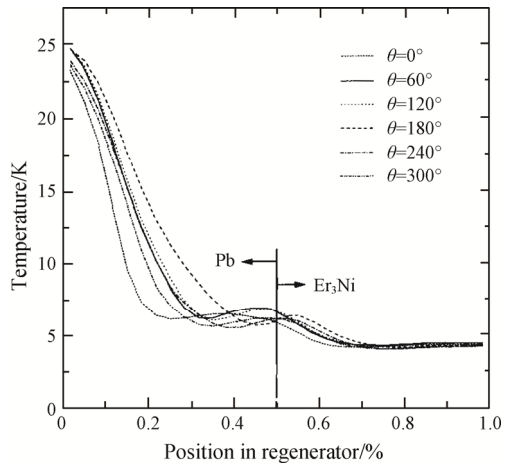

Fig. 6 Temperature distribution of the regenerative material at different times (noted as the phase angle of the pressure wave θ) during one cycle [29]

The possible value of the heat conduction and the heat-associated enthalpy flow was calculated, so as to determine the main term that keeps the energy balance.

The pressure-induced enthalpy flow is related to the parameter $(1–T\beta)$ together with the compressibility factor, as expressed in Eq. (1). The pressure-induced enthalpy flow dominates the energy imbalance because it varies drastically with the temperature. This value can be larger than the PV power at the cold end, as found in these publicly reported cases [38–40]. Here shows one example of an ideal regenerator that works at a temperature range of 4.2 K to 20 K. The theoretical value of the heat-associated enthalpy flow plus the heat conduction increases from the minimum value of close to zero to the maximum value of 2.75 times of the PV power at the cold end, as shown in Fig. 7.

The magnitude of heat conduction was found [14] to be about tens of milliwatt, which is only one-tenth or even one-hundredth of the magnitude of the variation of the pressure-induced enthalpy flow in these publicly reported cases [38–40].

Meanwhile, the heat-associated enthalpy flow was found [14] to have a magnitude that is comparable with the pressure-induced enthalpy flow. It was calculated based on the definition of the heat-associated enthalpy flow.

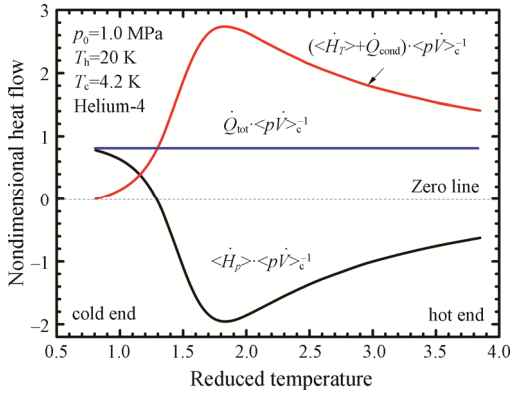

Fig. 7 Example of the distribution of the nondimensional energy flow terms (normalized by the PV power at the cold end) in the regenerator. The black, blue and red line represents for the pressure-induced enthalpy flow, the total heat flow and a sum of the heat-associated enthalpy flow and the heat conduction, respectively. A typical case of ^{4}He at a pressure of 1.0 MPa is selected as the example. The hot-end and cold-end temperature is equal to 20 K and 4.2 K, respectively.

This means that the heat-associated enthalpy flow should be the main factor, while the heat conduction should be a minor factor. The heat conduction can even be neglected, so as to simply the deduction.

But why the temperature gradient is much related to the heat-associated enthalpy flow? A scrupulous derivation [14] showed that there is a proportional relationship between these two parameters.

This relationship provided a theoretical basis for analyzing the nonlinear temperature profile of the regenerator. The differential equation [14] that determines the temperature profile was expressed as:

$$\frac{\left\langle p\dot{V}\right\rangle_{\mathrm{h}}}{(ZT)_{\mathrm{h}}}\frac{\mathrm{d}\left[(1-T\beta)ZT\right]}{\mathrm{d}x} - k_T\frac{\mathrm{d}^2T}{\mathrm{d}x^2} = 0 \tag{6}$$

And the coefficient between the heat-associated enthalpy flow and the temperature gradient is a complex combination of the internal parameters of gas and matrix [14], which was expressed as:

$$k_T = -\frac{0.5946}{\pi^{1.3}} \cdot \frac{\left(\frac{1}{\tau}(1-\phi)\rho_{\mathrm{m}}c_{p,\mathrm{m}} + h_{\mathrm{ht}}\phi / d_{\mathrm{h}}\right) c_{p,\mathrm{g}} d_{\mathrm{h}}^{1.3} Pr^{2/3} \cos\delta \left\langle p\dot{V}\right\rangle^{0.65}}{\left(\frac{1}{\tau}(1-\phi)\rho_{\mathrm{m}}c_{p,\mathrm{m}}\right) a_2 \mu^{0.3} \phi^{0.3} d_{\mathrm{reg}}^{0.6} \left(Zv\cos(\varphi-\theta)\right)^{0.65}} \tag{7}$$

where a_2, d_{h}, Pr, ϕ, and μ are nondimensional parameters related to matrix porosity, the hydraulic diameter of the matrix, the Prandtl number, matrix porosity, and the dynamic viscosity, respectively. What's more, δ, φ, and θ are the phase difference between the mass flow and the temperature, the phase of the mass flow, and the phase of the pressure, respectively.

The calculated temperature profiles at various cold-end temperatures are shown in Fig. 8. It is clear that these profiles are reasonably close to the measured ones [34], as shown in Fig. 5, although the calculation was based on a theoretical regenerator where there is no flow resistance and the coefficient k_T was assumed to be constant in that temperature range.

We would conclude that these analyses uncovered both the loss terms and the peculiar temperature profile in the regenerator with reasonable explanations.

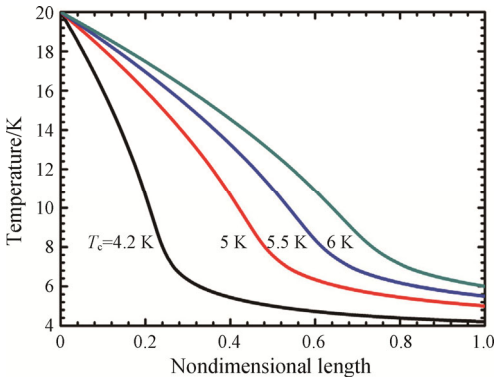

Fig. 8 Calculated temperature profiles of the regenerator [14]. The gas is ^{4}He. The pressure is 0.92 MPa and the hot-end temperature is fixed as 20 K. The black, red, blue, and cyan line represents a cold-end temperature of 4.2 K, 5 K, 5.5 K, and 6 K, respectively.

2.2 Determination of the COP

How large the theoretical COP is important for the cognition of real gas effects and also for estimating the performance of practical hardware.

Some researchers have realized that the pressure-induced enthalpy flow at the cold end should not be used to calculate the COP [13, 41], because the COP will exceed the Carnot COP in some temperature range where the pressure-induced enthalpy flow is negative. The pressure-induced enthalpy flow was the maximum one of that at the cold end and the hot end [13, 41], as shown:

$$\left\langle \dot{H}_p \right\rangle = \max\left(\left\langle \dot{H}_p \right\rangle_{\mathrm{c}}, \left\langle \dot{H}_p \right\rangle_{\mathrm{h}}\right) \tag{8}$$

The COP of a PTR that the expansion work is dissipated was expressed as:

$$\mathrm{COP} = \frac{(ZT)_{\mathrm{c}} - \left\langle \dot{H}_p \right\rangle / \left\langle p\dot{V} \right\rangle_{\mathrm{c}}}{(ZT)_{\mathrm{h}}} \tag{9}$$

The explanation that the hot-blow stream should be warmer than the cold-blow stream is reasonable [13]. It is a pity that the loss related to the temperature difference was not analyzed, and thus the physical meaning of the heat-associated enthalpy flow was not clear enough. What's more, it is a violation of physical law that to directly use the hot-end pressure-induced enthalpy flow $\left(\left\langle \dot{H}_p \right\rangle_{\mathrm{h}}\right)$ when analyzing the cold-end performance.

In order to solve that issue, the following equations were deduced [42]. The local pressure-induced enthalpy flow at the cold end was used for calculating the refrigeration power.

The heat conduction that is in very small magnitude was neglected, and the maximum net refrigeration power available at the cold end of the regenerator could be expressed as:

$$\dot{Q}_{\mathrm{c}} = \left\langle p\dot{V} \right\rangle_{\mathrm{c}} - \left(\left\langle \dot{H}_p \right\rangle_{\mathrm{c}} + \left\langle \dot{H}_T \right\rangle_{\mathrm{c}}\right) \tag{10}$$

The heat-associated enthalpy flow at the cold end was determined with this equation:

$$\left\langle \dot{H}_T \right\rangle_{\mathrm{c}} = \left\langle \dot{H}_p \right\rangle_{\max} - \left\langle \dot{H}_p \right\rangle_{\mathrm{c}} \tag{11}$$

because the heat-associated enthalpy flow equals to zero at the point where the pressure-induced enthalpy flow reaches its maximum of that regenerator section.

Therefore, the net refrigeration power was expressed as:

$$\dot{Q}_{\mathrm{c}} = \left\langle p\dot{V} \right\rangle_{\mathrm{c}} - \left\langle \dot{H}_p \right\rangle_{\max} \tag{12}$$

It is clear that the net refrigeration power at the cold end is reduced by the magnitude of the maximum pressure-induced enthalpy flow in that regenerator.

Regarding an ideal regenerative refrigerator, there should be an ideal isothermal compression and an ideal isothermal expansion at the hot end and cold end of the regenerator [7], respectively, so the COP of regenerator was expressed as:

$$\mathrm{COP} = \frac{(ZT)_{\mathrm{c}} - \max\left[(1-T\beta)ZT\right]}{(ZT)_{\mathrm{h}} - (ZT)_{\mathrm{c}}} \tag{13}$$

The relative Carnot COP (rCOP) for ^{4}He and ^{3}He at the pressure range of 0.5 MPa to 2.5 MPa was calculated

and was plotted in Fig. 9 [42]. It showed that the COP is always smaller than the Carnot COP. It was found that the theoretical COP for ^{4}He between a temperature below about 5 K and 20 K increases with the pressure. For example, the theoretical COP at 2.5 MPa is 50% higher than that at 1 MPa. That is different from a common idea that the pressure should be about 1 MPa [13, 43, 44] when the refrigeration temperature is around 4 K. The main reason is that the compressibility factor below about 5 K decreases sharply when the pressure decreases (as shown in Fig. 2), while the compressibility factor at the hot end (20 K, T_r=3.85 for ^{4}He) is close to unity at various pressures. The maximum value of the combined factor $(1-\beta T)ZT$ in that temperature range increases quickly with the pressure. In this case, the denominator of the expression of the COP decreases as the pressure increases, and the numerator increases, so the COP increases steadily with the pressure.

It was emphasized that the COP of PTRs is larger than that of working with an ideal gas in some temperature ranges [13, 41], as shown in Fig. 10. The cold-end temperature is in the range of around 10 K to 20 K where the pressure-induced enthalpy flow is negative all around that temperature range. Here we give an explanation. It is because the unrecovered expansion work in the refrigerator working with a real gas is smaller than that working with an ideal gas. Note that the refrigeration power for a real gas is larger than that of an ideal gas, which is beneficial to enhance the refrigeration density. However, the COP is still smaller than that working with an ideal gas (i.e. Carnot COP) if the expansion work is taken into account [42], so it is not against the second law of thermodynamics.

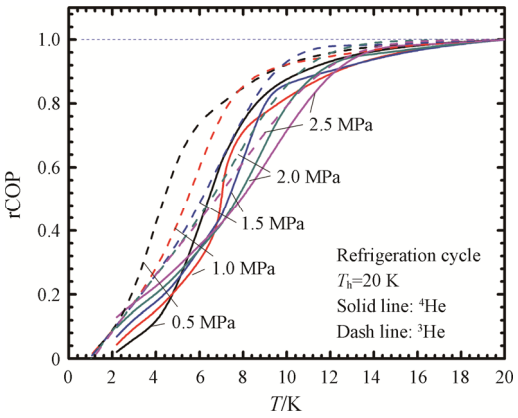

Fig. 9 Dependence of the relative COP of the refrigerator cycle on the cold-end temperature [42]. The hot-end temperature is set to be 20 K; the cold-end temperature goes down to 2.2 K and 1.0 K for ^{4}He and ^{3}He, respectively. The black, red, blue, cyan, and magenta lines represent a pressure of 0.5 MPa, 1.0 MPa, 1.5 MPa, 2.0 MPa and 2.5 MPa, respectively.

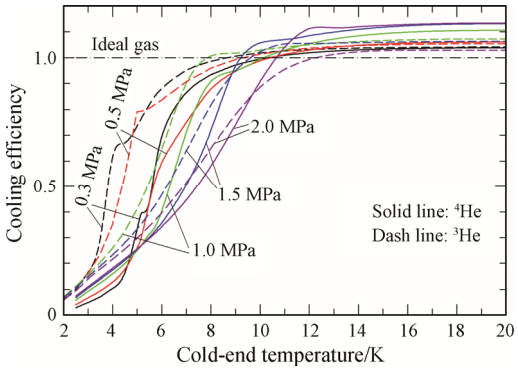

Fig. 10 Ratio of theoretical COP working with a real gas to that working with an ideal gas for a perfect last stage of a regenerative refrigerator without a recovery of the expansion work [13]. The hot-end temperature is set to be 20 K, and the cold-end temperature goes down to 3 K and 2 K for ^{4}He and ^{3}He, respectively. The black, red, green, blue, and purple lines represent a pressure of 0.3 MPa, 0.5 MPa, 1.0 MPa, 1.5 MPa, and 2.0 MPa, respectively.

2.3 Loss mechanism in the regenerator

The rCOP gets down to below about 30% when the refrigeration temperature is below the critical point [13, 42], as shown in Fig. 9, where the pressure-induced enthalpy flow accounts for more than 50% of the local PV power. It is generally regarded that the pressure-induced enthalpy flow brings about the loss itself.

We will clarify in this paper that this loss stems from the entropy generation related to the heat-associated enthalpy flow rather than the pressure-induced enthalpy flow itself, and the entropy generation is distributed throughout the regenerator.

The entropy flow in the regenerator has been derived based on the definition of the entropy and it is related to the properties of real gas effects [45], which is expressed as

$$\frac{\langle \dot{S} \rangle}{\langle p\dot{V} \rangle_h / (ZT)_h} = \frac{1}{T}\left\{ \left[(1-T\beta)ZT \right]_{\max} - ZT \right\} \tag{14}$$

where $\langle \dot{S} \rangle$ is the time-averaged entropy flow.

The characteristic entropy generation at any temperature interval is expressed as

$$\frac{1}{\langle p\dot{V} \rangle_h / (ZT)_h} \frac{\mathrm{d}\dot{S}_{\mathrm{gen}}}{\mathrm{d}T} = \frac{1}{T^2}\left[(1-T\beta)ZT \right]_{\max} + \frac{\mathrm{d}Z}{\mathrm{d}T} \tag{15}$$

The entropy flow in the regenerator is generally negative, while the entropy generation is always nonnegative. For example, the distribution of entropy generation per unit temperature at a typical temperature range from 4.2 K to 20 K and at a reduced pressure of 4.0 (0.91 MPa) is shown in Fig. 11. The entropy generation

at the peak point of the pressure-induced enthalpy flow, which is at the cold end for this case, is equal to the minimum value of zero. The entropy generation reaches its maximum value at the bottom point of the pressure-induced enthalpy flow, i.e. the peak point of the heat-associated enthalpy flow.

However, the entropy generation at a certain temperature is not stationary, even though the pressure-induced enthalpy flow is a constant. If the refrigeration cycle is limited to a smaller range, the entropy generation will decrease accordingly. For example, at a temperature range of 8 K to 10 K and 12 K to 16 K, the peak entropy generation rate is 13% and 27% of that at the temperature range of 4.2 K to 20 K, respectively. It is clear that the entropy generation at these small temperature ranges is significantly reduced, as shown in Fig. 11. Furthermore, if the cold-end temperature and the hot-end temperature in the refrigeration cycle are indefinitely close to each other, the entropy generation will decrease indefinitely, and the heat-associated enthalpy flow will also become infinitely small (close to zero), no matter how large the pressure-induced enthalpy flow is.

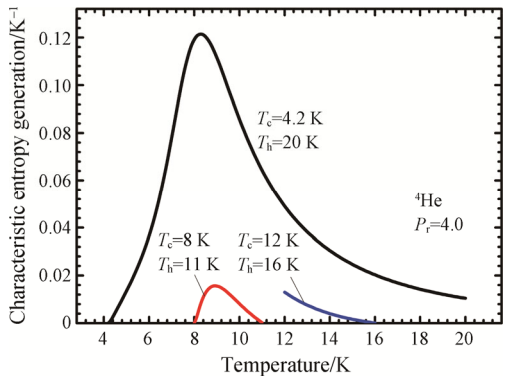

Fig. 11 The characteristic entropy generation along the regenerator temperature profiles under typical operating conditions. ^{4}He at a reduced pressure of 4.0 (0.91 MPa) is taken as the example. The black, red, and blue line represents a working temperature range of 4.2 K to 20 K, 8 K to 11 K, and 12 K to 16 K, respectively.

Consequently, the COP of the refrigeration cycle increases as the temperature range gets reduced, which is easily calculated with previous equation of the COP. The rCOP at the temperature range of 8 K to 11 K and 12 K to 16 K reaches 92.9% and 93.8%, respectively. Furthermore, if the temperature range of the refrigeration cycle gets close to 0.1 K, the rCOP is above 98%, even at a temperature range of 4 K to 4.1 K where the real gas effects are extremely serious. If the temperature range in the refrigeration cycle is indefinitely small, the rCOP will get indefinitely close to 100%. This demonstrates that the serious real gas effects themselves do not directly mean any loss. This means that even though the absolute value of the pressure-induced enthalpy flow is quite large, it will not bring about a heat-associated enthalpy flow.

In fact, it is the variation of the real gas effects (i.e. the variation of pressure-induced enthalpy flow) at the temperature range of the regenerator that brings about the heat-associated enthalpy flow, and such a heat-associated enthalpy flow brings about an entropy generation (i.e. heat loss). We will conclude that real gas effects indirectly give rise to the heat loss in the regenerator, which is renewed from the previous cognition.

2.4 Ultimate temperature of the regenerative refrigeration

There will be no refrigeration effect if the volume expansivity equals to zero [9, 46, 47]. This principle applies to any refrigeration system that relies on an adiabatic expansion to generate a refrigeration power. Zero volume expansivity means that the pressure-induced enthalpy flow equals to the local PV power, when the temperature is around a reduced temperature of 0.5, as shown in Fig. 3.

This point determines the ultimate temperature that the working gas is capable to achieve. Pursuing the lowest temperature has been a splendid work when the regenerative refrigerator was able to achieve 4.2 K in the middle 1990s [33]. The theory has provided an important guide for this.

The zero point of volume expansivity decreases slowly as the pressure increases for ^{4}He, which is close to the lambda line of ^{4}He, as shown in Fig. 12. The experimental study got a minimum temperature of 2.13 K with a PTR [48], which is 0.19 K above the lambda line of ^{4}He at that average pressure of 1.95 MPa. Actually, it

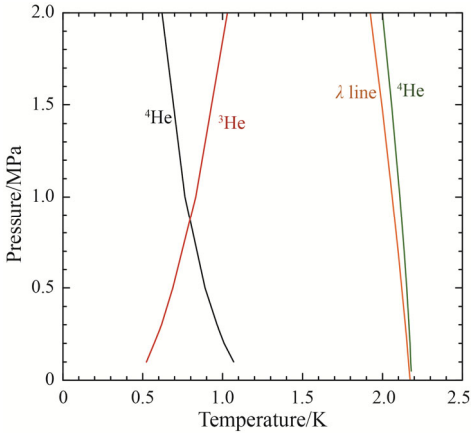

Fig. 12 The locus in pressure-temperature space where the cooling power of an ideal PTR is zero for ^{4}He and ^{3}He working fluids. Also shown is the lambda line of ^{4}He [47]

is only 0.13 K above the zero point of the volume expansivity, which shows an excellent experiment work of those authors. Although ^{4}He regains the ability to expand when the temperature gets lower than 1 K, the coefficient is too small to take its effects in practice [47]. There was a suggestion [49] that using a compression process instead of an expansion process to gain a refrigeration effect when the temperature is below 2 K, where ^{4}He actually becomes a superfluid. It was shown that a temperature drop of about 0.1 K is achieved with a pressure ratio of about 2. However, this cycle is difficult to put into practice, and there have been no reported experimental results ever since then.

The zero point of volume expansivity of ^{3}He gets down to 1 K, which is a significant advantage at this temperature range. Two laboratories in Europe charged the precious ^{3}He instead of ^{4}He in their GM-type PTRs, and got a temperature of below 2 K [50]. The record is 1.27 K when the mean pressure is 0.92 MPa [50], and it is only 0.32 K above the theoretical limit. Note that the zero point even extends to as low as 0.5 K when the pressure is as low as 0.1 MPa, as shown in Fig. 12. Experiments on Stirling-type PTR working with ^{3}He were reported [51, 52]. A maximum improvement of 0.9 K of the no-load refrigeration temperature was measured [51], comparing with that working with ^{4}He. Recent experimental study has achieved a lowest temperature of 3.47 K with ^{4}He [53], which is close to the lowest temperature of 3.0 K achieved with a Stirling-type refrigerator working with ^{3}He [54].

The expansion limit of the dilute ^{3}He in the fixed ^{4}He background is the phase separation of the mixture because the chemical potential varies as the concentration proceeds [47]. There seems to be no temperature limit when using such a mixture as a working fluid, if the concentration gets well-adjusted [47]. Experimental measurements have achieved a lowest temperature of 0.168 K [55], and it was calculated that a refrigeration power of 40 μW at 0.1 K can be obtained [56]. Note that they applied a recuperator instead of a regenerator, and there are no fundamental differences of energy flow between regenerative and recuperative heat exchangers when only time-averaged behavior is considered [57]. However, the refrigeration power density is very small, which sets an obstacle to put such sub-kelvin refrigerators into practice applications.

2.5 Real gas effects on the pulse tube

There are relatively few studies on the real gas effects on the pulse tube or on the clearance gap. For example, the expansion efficiency of the pulse tube is usually estimated with an empirical value of 80%, which is based on a limited number of measurement at liquid-nitrogen temperatures [7, 58], while the expansion efficiency at lower temperatures has not been measured so far.

The ideal pulse tube is considered to be in an adiabatic process with sufficient flow strengthening and no heat exchange between the fluid and the wall. According to the first law of thermodynamics, the enthalpy flow in the pulse tube is equal to the PV power [7]. Since the flow resistance in the pulse tube is negligible, both the enthalpy flow and the PV power remain constant along the length. Given this, we can conclude that an ideal pulse tube is able to work with a real gas, because there is no violation of the energy-balance principle. In contrast, an ideal regenerator without any heat loss cannot work with a real gas [14, 35].

However, there is a heat transfer between the gas and the wall in a practical pulse tube, causing a heat loss ($\dot{Q}_{\text{loss}}$) and resulting in a degradation of enthalpy flow ($\langle \dot{H} \rangle$) further. The energy equation inside the pulse tube is expressed as follows:

$$\langle p\dot{V} \rangle = \langle \dot{H} \rangle + \dot{Q}_{\text{loss}} \tag{16}$$

According to the definition of the expansion efficiency of the pulse tube, i.e. the ratio of the enthalpy flow to the PV power at the cold end, the heat exchange between the gas and the wall obviously reduces the efficiency of the pulse tube.

It has long been ambiguous whether the enthalpy flow includes the pressure-induced enthalpy flow or not. We would say that, since both the temperature and the pressure varies as the gas flows through the tube, the pressure-induced enthalpy flow always exists only if there is a PV power and the working fluid is of a real gas, according to its definition.

Similar to the situation in the regenerator, the heat-associated enthalpy flow in the pulse tube is also adjusted as the variation of the pressure-induced enthalpy flow, as shown in Fig. 13. Note that the heat-associated enthalpy flow is directly related to the heat loss in the pulse tube, because the temperature amplitude of the gas results in a heat transfer between the gas and the wall.

The pressure-induced enthalpy flow of ^{4}He is close to the PV power at the liquid-helium temperature, and then the heat-associated enthalpy flow gets small. In this case, the heat loss decreases, and the expansion efficiency of the pulse tube increases. The pressure-induced enthalpy flow is negative when the temperature is between about 10 K and 30 K, and the heat-associated enthalpy flow is possible to exceed the PV power, so the heat loss increases and the expansion efficiency of the pulse tube decreases. For example, at a typical temperature range of 4 K to 20 K for an average pressure of 1.0 MPa, the heat-associated enthalpy flow at the cold end is only 20% of the PV power, comparing to twice the PV power at about 9 K, as shown in Fig. 13. Obviously, the heat loss at these two places is significantly different.

Note that the connection between the heat exchanger

and the adiabatic part leads to a heat loss at both the cold and hot ends of the pulse tube, and there is a possible jet loss due to insufficient flow strengthening in hardware. These factors increase the complexity of the problem of determining the expansion efficiency. However, these studies are still very limited, with only a few numerical simulations [59, 60].

The temperature profile of the pulse tube is strongly influenced by the heat-associated enthalpy flow, and it is found to be far from linear when the real gas effects are significant, just like that in the regenerator. It was found that about 95% of the temperature variation happens in the 40% of the whole length that near the hot end. This was carried out through an experimental measurement [33, 61] and a numerical analysis [29, 61], in a case of the GM-type PTR working down to 4 K, as shown in Fig. 14. This means that the heat exchange happens most near the hot end of the pulse tube. Note that there was possible a DC flow in the PTR, because a double inlet worked as the phase shifter [29, 33].

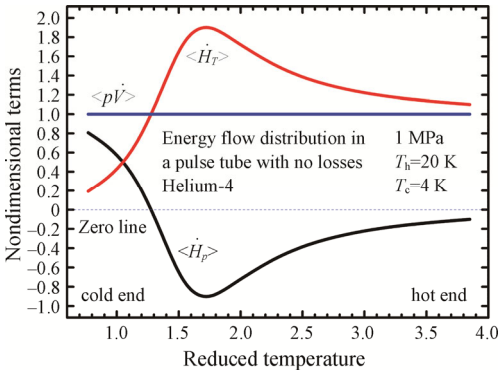

Fig. 13 Variation of the energy flow terms against the reduced temperature in an ideal pulse tube. The cold-end and hot-end temperature is 4 K and 20 K. The pressure is 1 MPa. The black, red, and blue line represents the nondimensional terms (divided by the PV power) of the pressure-induced enthalpy flow, the heat-associated enthalpy flow, and the PV power, respectively.

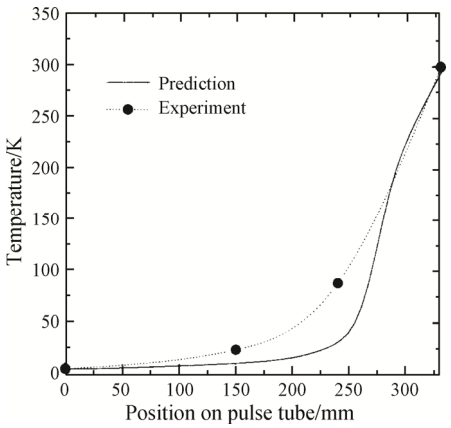

Fig. 14 Numerical simulation and experimental measurement of the temperature profile of a pulse tube in a GM-type PTR [29]

3. Method Studies of Reducing Real Gas Losses

Although the real gas losses are serious, they have been long regarded as an "intrinsic" loss and cannot be reduced [13, 18, 25, 35, 36]. The reason is mainly that it is the physical properties of the gas that determine the variation of pressure-induced enthalpy flow and there is no method to alter the properties.

Fortunately, there have been sporadic studies on reducing real gas losses, even though some researchers didn't even realize this. The regenerator at liquid-helium temperatures was found to provide an intermediate refrigeration power at an intermediate temperature between the cold-end temperature and hot-end temperature [62–64], which was extracted in the middle section of a regenerator, leading to little or no degradation on the refrigeration performance at the cold end (at about 4 K). The intermediate refrigeration power was ever called "excess cooling power" [64] or "free cooling power" [63], which shows its characteristic. The energy flow in the regenerator has been theoretically analyzed [64], and it was clearly demonstrated that the enthalpy flow at the upper part of the regenerator is reduced when an intermediate refrigeration power is applied [64], shown as a drop from 4.12 W down to 1 W in Fig. 15. In other words, the "enthalpy loss" somehow turns into the intermediate refrigeration power in that theoretical model [64].

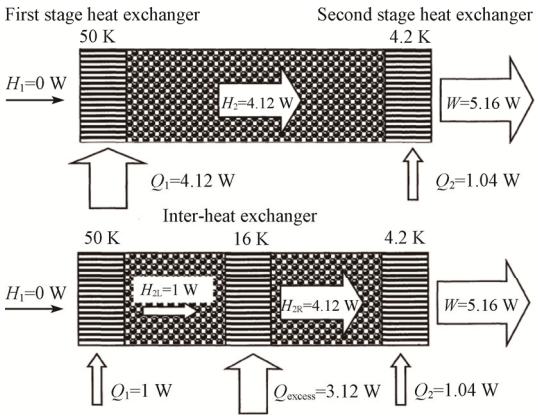

Fig. 15 Theoretical comparison of the energy flow in a perfect second-stage regenerator that without and with an inter-heat exchanger [64]. The notations of Q_{excess}, Q_1, and Q_2 refer to the refrigeration power of the intermediate part, the first stage and the second stage, respectively. The notations of H_1, H_2, H_{2L} and H_{2R} refer to the enthalpy flow of the first stage, the second stage (without the inter-heat exchanger), the left part and the right part of the inter-heat exchanger, respectively. The work at the cold end is set as a constant.

The experiments have shown a variable intermediate refrigeration power at that variable intermediate temperature [63], as shown in Fig. 16. For example, 0.5 W at 5.9 K or 1.25 W at 7.9 K was measured, as shown in Fig. 17, which is comparable with or even larger than the refrigeration power at the cold end of the second stage.

These analyses and experiments have illustrated that the real gas losses are able to reduce. It is a pity that there were only limited experimental measurements and numerical analyses. The physical mechanism of these methods has been expounded with a theoretical derivation in the year later [65], as described below. The research about applying a DC flow in the regenerator and the expansion components will be further described.

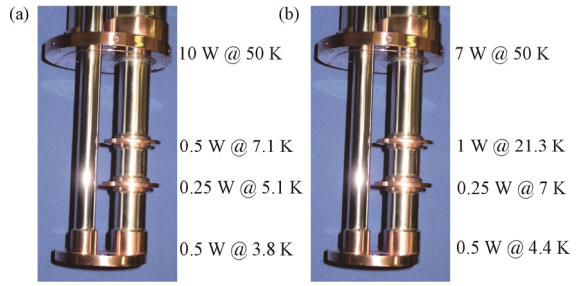

Fig. 16 Figure of the experimental setup of a two-stage PTR and tested results [63]. Two intermediate heat exchangers were anchored in the middle of the regenerator.

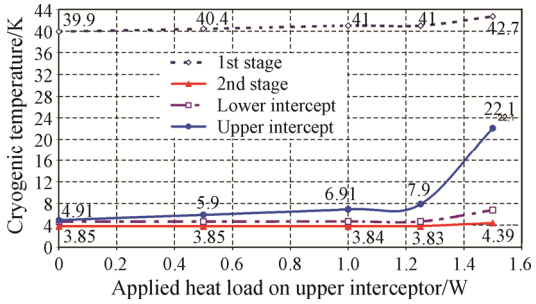

Fig. 17 Measured intermediate refrigeration power in a two-stage PTR. The red, dash blue, and solid blue line represents the second-stage, first-stage, and intermediate refrigeration temperature. The horizontal axis represents the intermediate refrigeration power. There is 0.5 W heat load on the second stage, but no load on the first stage [63].

3.1 Theory of heat input or removal in the regenerator

The regenerator was assumed to be one-dimensional, frictionless, and without axial conduction. Furthermore, there could be an infinite heat-transfer rate and infinite matrix heat capacity at any point whenever it is possible [14, 65]. These assumptions should avoid any disturbance of practical factors such as heat-transfer limitation or flow friction. The regenerator is possible to be lossless in an ideal case.

A differential heat input or removal was carried out all along the regenerator [65], as illustrated in Fig. 18. Such a heat input or removal is fully related to the real gas properties, as expressed here:

$$\frac{\delta\dot{Q}\Big/\left\langle p\dot{V}\right\rangle_{\mathrm{h}}}{\delta T}=\frac{1}{(ZT)_{\mathrm{h}}}\frac{\mathrm{d}\left[(1-T\beta)ZT\right]}{\mathrm{d}T} \tag{17}$$

This equation defines the distributed intermediate refrigeration power or intermediate heat input. If the coefficient of the pressure-induced enthalpy flow at the local point is smaller than that at a colder point, it is a heat input; and in the other case where the coefficient at the local point is larger than that at a colder point, it is a heat removal, as shown in Fig. 18.

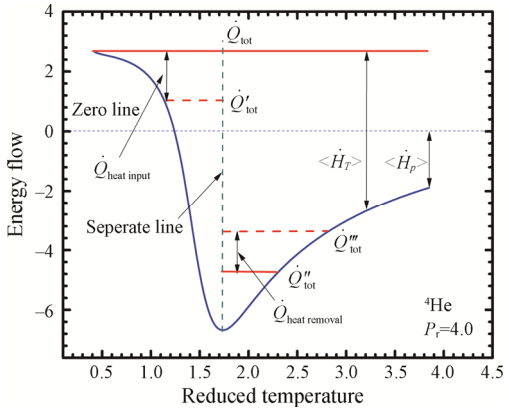

Fig. 18 Illustration of the heat input or removal theory in an ideal regenerator. A typical case of ^{4}He at a reduced pressure of 4.0 is selected as the example. The blue and red lines represent for the pressure-induced enthalpy flow and the total heat flow, respectively. The dash red lines represent the total heat flow above the point that the heat input or removal is applied. The difference of the red line and blue line equals to the integration of the local differential heat input or removal. The cyan dash line represents the separation of the region where heat input should be applied and the region for the heat removal.

The heat-associated enthalpy flow brought about by the pressure-induced enthalpy flow was then further converted into the available energy by assuming numerous numbers of microcycles between the hot-end temperature and the local temperature [65]. In this way, all heat loss was recovered, and a COP was obtained in an ideal case, which was expressed as:

$$\mathrm{COP}=\frac{(ZT)_{\mathrm{c}}}{(ZT)_{\mathrm{h}}}\times\frac{(\beta T)_{\mathrm{c}}}{1-\dfrac{(ZT)_{\mathrm{c}}}{(ZT)_{\mathrm{h}}}-\displaystyle\int_{T_{\mathrm{c}}}^{T_{\mathrm{h}}}\frac{(T_{\mathrm{h}}-T)}{T(ZT)_{\mathrm{h}}}\frac{\mathrm{d}\left[(1-T\beta)ZT\right]}{\mathrm{d}T}\mathrm{d}T} \tag{18}$$

The numerous numbers of microcycles can also be

built between the cold-end temperature and the local temperature, so all heat loss is converted into the refrigeration power at the cold end, requiring some input power, and the COP is expressed in another form:

$$\mathrm{COP}=\frac{(ZT)_{\mathrm{c}}(\beta T)_{\mathrm{c}}+(ZT)_{\mathrm{h}}\int_{T_{\mathrm{c}}}^{T_{\mathrm{h}}}\frac{T_c}{T(ZT)_{\mathrm{h}}}\frac{\mathrm{d}\left[(1-T\beta)ZT\right]}{\mathrm{d}T}\mathrm{d}T}{(ZT)_{\mathrm{h}}-(ZT)_{\mathrm{c}}+(ZT)_{\mathrm{h}}\int_{T_{\mathrm{c}}}^{T_{\mathrm{h}}}\frac{T-T_{\mathrm{c}}}{\mathrm{T}(ZT)_{\mathrm{h}}}\frac{\mathrm{d}\left[(1-T\beta)ZT\right]}{\mathrm{d}T}\mathrm{d}T} \tag{19}$$

By calculating cases working with ^{4}He and ^{3}He [65], it demonstrated that the Carnot efficiency could be obtained with this method, at any pressure or at any temperature.

This distribution method was then further simplified by exerting such a heat input or removal at discrete regenerator locations [65], which was solved by an integration:

$$\dot{Q}_i=\int_{T_{i-1}}^{T_i}\frac{\langle p\dot{V}\rangle_{\mathrm{h}}}{(ZT)_{\mathrm{h}}}\frac{\mathrm{d}\left[(1-T\beta)ZT\right]}{\mathrm{d}T}\mathrm{d}T \tag{20}$$

The COP of the discrete method was expressed as:

$$\mathrm{COP}=\frac{(ZT)_{\mathrm{c}}(\beta T)_{\mathrm{c}}+\sum_{i=1}^{n}\frac{T_{\mathrm{c}}}{T_i}\int_{T_{i-1}}^{T_i}\frac{\mathrm{d}\left[(1-T\beta)ZT\right]}{\mathrm{d}T}\mathrm{d}T}{(ZT)_{\mathrm{h}}-(ZT)_{\mathrm{c}}+\sum_{i=1}^{n}\frac{T_i-T_{\mathrm{c}}}{T_i}\int_{T_{i-1}}^{T_i}\frac{\mathrm{d}\left[(1-T\beta)ZT\right]}{\mathrm{d}T}\mathrm{d}T} \tag{21}$$

Although there is some finite heat loss, still 90% of the Carnot efficiency was obtained, when a heat input of 7 discrete regenerator locations, which were equidistribution of temperature, was applied in some certain temperature range both for ^{4}He and ^{3}He [65], as shown in Fig. 19. The improvement with a single location is still significant, which added to 41% of the Carnot efficiency.

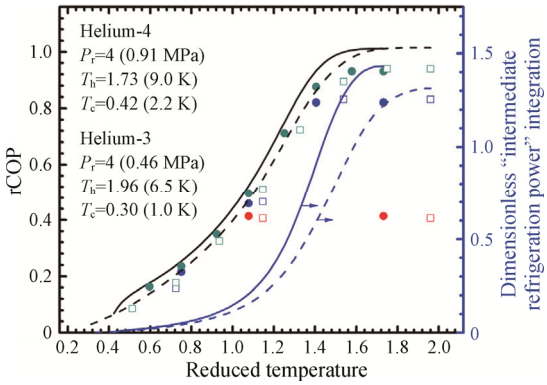

Fig. 19 The relative Carnot COP taking into account the "intermediate refrigeration power" [65]. The reduced pressure is 4.0; the hot-end temperature (reduced temperature) is 1.73 for ^{4}He and 1.96 for ^{3}He, and the cold-end temperature (reduced temperature) is 0.42 for ^{4}He and 0.30 for ^{3}He. The solid line and solid points represent for ^{4}He, and the dash line and hollow points represent for ^{3}He. The black lines are the distributed cases. The red, blue, and cyan points represent for the discrete cases of 1 location, 3 locations, and 7 locations (equidistribution of temperature), respectively.

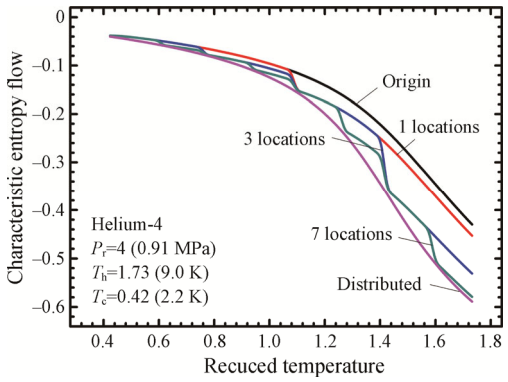

Fig. 20 The characteristic entropy flow in a regenerator taking into account the intermediate refrigeration power. The black and magenta line represents the original case (without heat input) and the distributed case. The red, blue, and cyan line represents for the discrete cases of 1 location, 3 locations, and 7 locations (equidistribution of temperature), respectively.

Here we analyze the entropy flow in the regenerator when various heat inputs were applied, as shown in Fig. 20. The entropy flow should be negative in this isothermal component according to the thermodynamics of oscillation flow [7]. The larger the absolute value of the entropy flow, the larger potential of the refrigeration power. It shows that the absolute value of the entropy flow gets larger when the heat input method was applied. The entropy flow decreases to a value equaling to that of the distributed method at the point of discrete heat input. With more points of the discrete method, the entropy flow gets closer to that of the distributed method. Note that there is no entropy generation at the point of discrete

heat input and also in the whole range of the distributed method.

It is reasonable to conclude that the intermediate refrigeration power [62–64] belongs to a simplified method of extracting a refrigerator power at discrete regenerator locations in a practical regenerator [65], as shown in Fig. 16. The more points of extracting such a refrigerator power, the larger improvement of the total refrigeration power. Note that there is a radial heat resistance in such a practical regenerator, and the regenerator efficiency is also limited, so the intermediate refrigeration power is smaller than the theoretical value.

It has been observed in experiments that the intermediate refrigeration power decreases the refrigeration power at the upper stage [62, 63], as shown in Fig. 17. It was also analyzed that the refrigeration power at the upper stage (50 K) drops from 4.12 W down to 1 W [64], as shown in Fig. 15. Here we uncover the internal mechanism that was simply illustrated in the previous study [64] by applying the heat input or removal theory across stages.

There are generally two types of staging methods for regenerative refrigerators, which are named as thermal coupling [66] and gas coupling [67]. They both have an energy interaction between stages, while there is a mass flow interaction in the gas-coupling method. However, the function of the upper stage provides both refrigeration power of present stage and part of precooled regenerator for its lower stage in the gas-coupling method, so the regenerator at the upper stage can be separated into two parts, from the view point of energy flow [67]. The energy analysis on the thermal-coupling method is adaptable to that of the gas-coupling method. An illustration of this analysis is shown in Fig. 21.

The precooling power for the lower stage is actually one kind of heat removal because the total heat flow decreases, while the refrigeration power is one kind of heat input, if the energy balance of one regenerator in its whole length is analyzed through the cold end to the hot

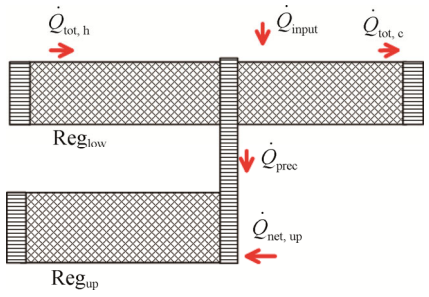

Fig. 21 Illustration of the heat input or removal theory across stages. The lower-stage regenerator (Reg_{low}) is precooled by the upper-stage regenerator (Reg_{up}) with a thermal coupling. The red arrows represent various heat flows.

end. The total heat flow is varied by means of integration of heat input and also the integration of heat removal, if the energy equation is expressed with a discrete method:

$$\dot{Q}_{\text{tot,c}} - \dot{Q}_{\text{tot,h}} = \sum \dot{Q}_{\text{input},i} - \sum \dot{Q}_{\text{removal},i} \tag{22}$$

This means that the variation of the heat removal is equal to the variation of the heat input, and in the case, the total heat flows at the two ends are fixed. Especially, there is only one point of heat removal, i.e. the precooling between stages, and the energy equation is expressed as:

$$\Delta\dot{Q}_{\text{prec}} = \sum \dot{Q}_{\text{input},i} \tag{23}$$

Here the total heat flow at the cold end and at the upper stage is fixed, since the cold-end and upper-stage temperature keeps constant in this case.

The net refrigeration power at the upper stage is equal to the gross refrigeration power minus the precooling power, expressed as:

$$\dot{Q}_{\text{net,up}} = \dot{Q}_{\text{gross,up}} - \dot{Q}_{\text{prec}} \tag{24}$$

Combining these equations, we have:

$$\Delta\dot{Q}_{\text{net,up}} = -\sum \dot{Q}_{\text{input},i} \tag{25}$$

It is clear that the loss of the net refrigeration power at the upper stage is equal to the sum of the heat input, i.e. the intermediate refrigeration power.

However, the loss of the net refrigeration power in practical regenerators is generally larger than that of the intermediate refrigeration power [62]. The main reason is that the average temperature of the regenerator gets increased as the intermediate refrigeration power is applied, and the viscosity coefficient increases, and thus the flow-friction loss aggravates [66].

3.2 DC flow method in the regenerator

The DC flow method is possible to reduce real gas losses in the regenerator. This method is related to the heat input or removal method because the sensible heat capacity of the DC gas functions as a distributed heat input.

There are actually two kinds of DC flow in the regenerator: one that flows inside the regenerator is named as the internal DC flow, and the other that flows outside the regenerator is named as the external DC flow, as shown in Fig. 22. A special circular internal DC flow (Fig. 22(a)) is generated in a circular path through the regenerator and pulse tube in the PTR. The typical internal DC flow and external DC flow that pass through the hot end to the cold end of the regenerator are shown in Fig. 22(b) and Fig. 22(c), respectively. The energy equations for these two kinds of DC flow are actually the same. The main difference is that the external DC flow generally works with a significant radial heat resistance in practice, which is assumed to be zero in theoretical analyses.

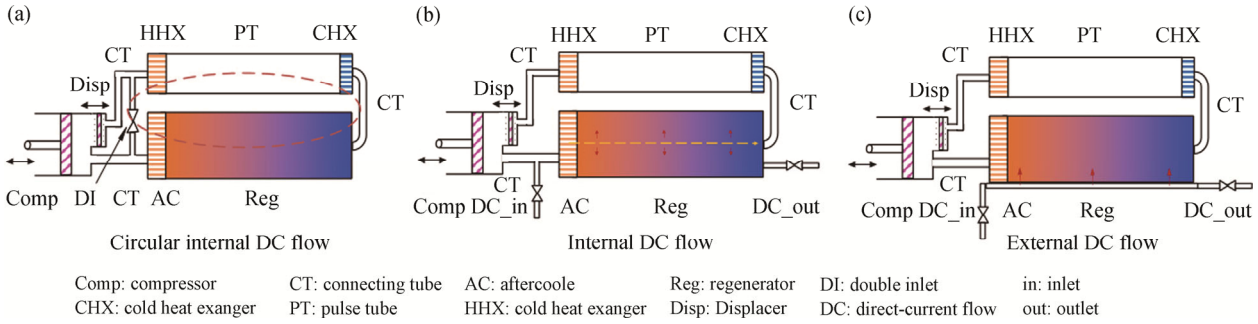

Fig. 22 Schematics of three kinds of DC flow that superimposed on the regenerator, a circular internal DC flow (a), an internal DC flow (b), and an external DC flow (c) (Adopted from [45] with permission from Elsevier).

The external DC flow is generally the gas to be liquefied, especially the helium gas. It was found that the liquefaction rate can be improved by precooling the gas outside the regenerator of 4 K PTR [68], which increased from 1.4 L/d to 4.8 L/d. The experimental setup is shown in Fig. 23. The numerical calculations demonstrated that the improvement of the liquefaction is caused by aid of the inefficiency of the regenerator [68].

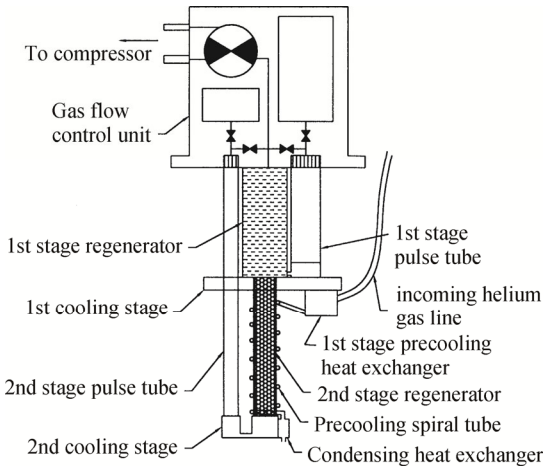

Fig. 23 Schematic of a two-stage PTR that precools the incoming tube outside the second-stage regenerator [68]

The real gas losses in the regenerator of the GM refrigerator are comparable with that of the GM-type PTR, but the radial conduction resistance at the gap is much larger because of the clearance gap [68]. Recent modifications, by removing low-conductivity layers and covering a plate over the outer wall to form a heat-convection passage, take effects and enable an improvement of liquefaction of 23.7% for ^{4}He [69].

The circular internal DC flow is widely applied in a doubled-inlet type PTR [70], as shown in Fig. 23. The performance has been improved significantly with an optimum internal DC flow flowing in a direction from the hot end of the regenerator to the cold end. Experiments showed that the DC flow improved the COP by 24% at 4.2 K [71], or the no-load temperature was decreased significantly down to 3.1 K for a GM-type PTR [32]. The refrigeration temperature was decreased by an order of 5 K at the temperature around 20 K in a Stirling-type PTR [72]. It was concluded that the DC flow brings about losses and should be zero when the refrigeration temperature gets down to as low as 24 K [73]. The value of the DC flow is very difficult to measure and it was generally described with the opening of the valve and monitored by measuring the temperature gradient of the pulse tube [32, 71, 74].

The DC flow has ever been precisely measured in recent years. It was done by measuring the pressure variation in a constant-volume reservoir, where the DC flow was induced through the refrigeration components [60, 75], as shown in Fig. 24. The amount of the DC flow was controlled precisely by controlling the valve before the DC reservoir. The refrigeration power was improved by over 1.5 times at 25 K when the DC flow was measured to be 2.1 mg/s [75], as shown in Fig. 25.

Note that when the DC flow was applied though both the regenerator and pulse tube in these experiments, the effects on these two components are actually synthetic. This makes it difficult to distinguish which component exerts the effects on the refrigeration performance [60, 76].

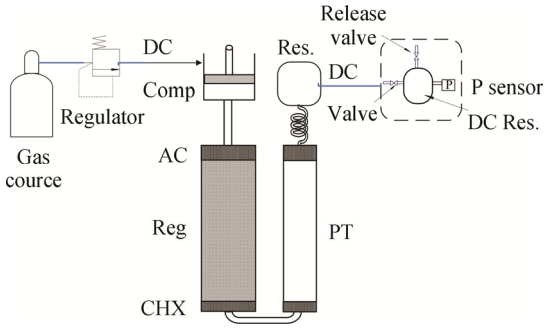

Fig. 24 DC flow measurement system in a PTR [75]

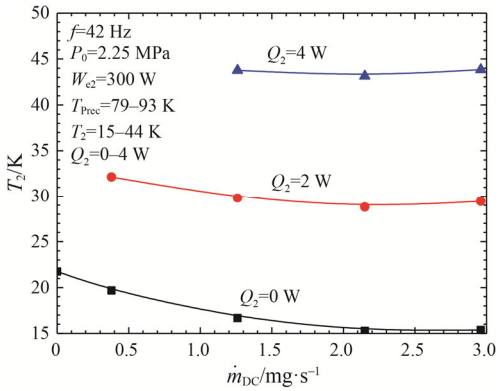

Fig. 25 Measured refrigeration temperature with various refrigeration power against the DC flow in a two-stage PTR [75]. The term W_{e2} means the input electrical power of the compressor for the second stage.

The working mechanism of the DC flow on the regenerator was explored in a theoretical model [45]. The assumption of the regenerator in this theoretical model is the same as that of the heat input or removal method, as discussed in Section 3.1 [45].

The energy balance of the regenerator with the DC flow was described with this equation:

$$\dot{Q}_{\text{tot}} = \left\langle \dot{H}_p \right\rangle + \left\langle \dot{H}_T \right\rangle + \dot{Q}_{\text{cond}} + \int_{T_c}^{T_x} \dot{m}_{\text{DC}} c_p \mathrm{d}T \tag{26}$$

Here the terms $\left\langle \dot{H}_p \right\rangle$, $\left\langle \dot{H}_T \right\rangle$ and $\dot{Q}_{\text{cond}}$ are functions of temperature (T_x), while the total heat flow $\dot{Q}_{\text{tot}}$ keeps constant. A schematic of this relationship is shown in Fig. 26.

In order to determine the maximum value of the DC flow that fulfills the energy balance at any location along the regenerator, a possible maximum DC flow in the temperature range between the cold-end temperature (T_c) and a variable higher temperature (T_x) was firstly solved [45], which means that the heat-associated enthalpy flow reaches a minimum value of zero at these two ends. So the energy balance is expressed as:

$$\dot{m}_{\text{DC},(T_c,T_x)} \int_{T_c}^{T_x} c_p \mathrm{d}T = \int_{T_c}^{T_x} \delta \left[(1 - T\beta) \left\langle p\dot{V} \right\rangle \right] \tag{27}$$

Secondly, the minimum value of the DC flow in that temperature range was determined by finding the minimum one in that group of DC flow [45], as shown that:

$$\dot{m}_{\text{DC,min}} = \min\left(\dot{m}_{\text{DC}}\right), T \in \left(T_c, T_h\right) \tag{28}$$

The DC flow recovers the distributed intermediate refrigeration power in the whole temperature range, which was converted to the refrigeration power at the cold end with microcycles. The COP of the regenerator that takes the DC flow into account was expressed as:

$$\text{COP} = \frac{(\beta T)_c (ZT)_c + \left(\dfrac{\dot{m}_{\text{DC,min}} (ZT)_h}{\left\langle p\dot{V} \right\rangle_h} \right) \int_{T_c}^{T_x} \dfrac{T_c}{T} c_p \mathrm{d}T}{(ZT)_h - (ZT)_c + \left(\dfrac{\dot{m}_{\text{DC,min}} (ZT)_h}{\left\langle p\dot{V} \right\rangle_h} \right) \int_{T_c}^{T_x} \dfrac{T - T_c}{T} c_p \mathrm{d}T} \tag{29}$$

It was found that the converted cold refrigeration power increases the rCOP from an order of 1% to 10% for cases of ^{4}He and ^{3}He [45], as shown in Fig. 27. This shows the significant improvement of the DC flow method.

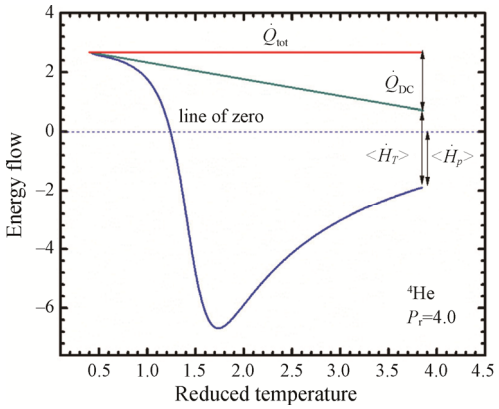

Fig. 26 Illustration of various energy flow terms in the regenerator at the temperatures close to or below the critical point [45]. The case of ^{4}He at a reduced pressure of 4.0 is taken as the example. The red, blue, cyan line represents the total heat flow, the pressure-induced enthalpy flow, and the sum of the pressure-induced enthalpy flow and the heat-associated enthalpy flow, respectively. The subtraction value between the cyan line and the blue line represents the heat-associated enthalpy flow. The subtraction value between the red line and the cyan line represents the enthalpy flow of the DC flow gas.

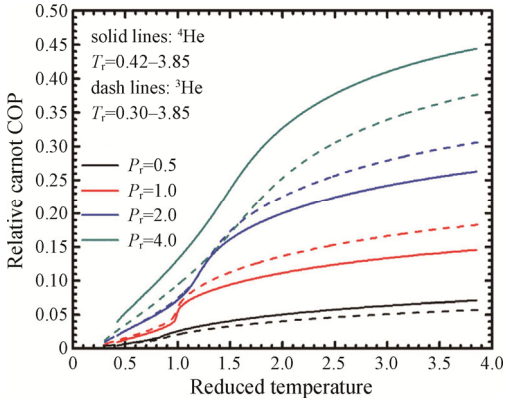

Fig. 27 The rCOP of ^{4}He and ^{3}He corresponding to various reduced pressures [45]. The minimum characteristic DC flow is applied and the effects are integrated from the cold end. The solid lines represent ^{4}He and the dash lines represent ^{3}He. The black, red, blue, and cyan lines represent the reduced pressure of 0.5, 1.0, 2.0, and 4.0, respectively.

The entropy flow of the regenerator was further analyzed [45]. The entropy flow decreases if the DC flow is applied, as shown in Fig. 28. The DC flow cannot eliminate all the entropy generation resulted from real gas effects, because the distributed enthalpy flow of the DC flow does not match the variation of the pressure-induced enthalpy flow completely. However, the minimum DC flow was found to increase if the hot-end and cold-end temperature gets closer, and the entropy generation decreases [45]. The entropy generation should approach zero as the two-end temperature difference gets indefinitely small.

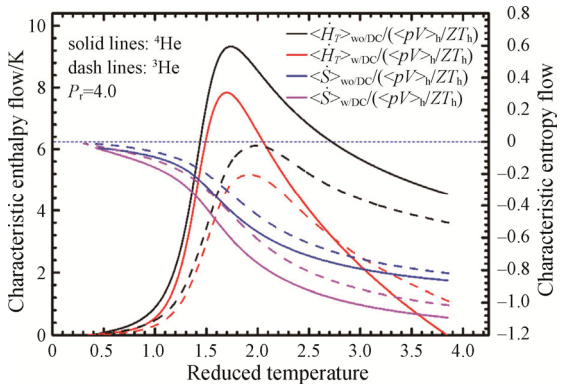

Fig. 28 Comparison of the characteristic enthalpy flow and the characteristic entropy flow in the regenerator without DC flow and with DC flow (indicated with subscripts of "wo/DC" and "w/DC") [45]. The reduced pressure is set as 4.0. The solid lines represent ^{4}He, and the dash lines ^{3}He. The black, red lines represent the enthalpy flow without DC flow and with DC flow, respectively. The blue, pink lines represent the entropy flow without DC flow and with DC flow, respectively.

3.3 Decreasing losses in the pulse tube

The circular internal DC flow (Fig. 22(a)) in the PTR generally flows through the regenerator to the pulse tube by way of the cold end, which is noted as a positive direction of the DC flow. The DC flow drawn from the regenerator has a distributed regeneration power, which has an effect on reducing the heat transfer loss in the pulse tube. The refrigeration performance is generally improved significantly when the cold-end temperature is in the range of liquid-helium temperature [32, 71, 76] and liquid-hydrogen temperatures [60, 72, 75], where the real gas effects are serious.

The mechanism investigation in public literatures on the circular internal DC flow in the PTR is closely related to the pulse tube. The explanations for the improvement at 4 K PTRs include that the DC flow increases the refrigeration capacity of the pulse tube and dissipates more of the enthalpy flow at the hot end of the pulse tube [76]. It was concluded that the induced DC flow is used to compensate the DC flow generated by the double-inlet valve [32]. Another explanation was that the DC flow varies the temperature gradient both in the pulse tube and the regenerator and makes it more reasonable, where the refrigeration temperature is around 20 K [60].

It is a pity that there were not much solid experimental data or theoretical data to support those conclusions. They cannot explain the difference between the influence at the liquid-helium temperatures and that at a higher temperature of above 80 K, i.e. the influence of real gas effects. What's more, the temperature profile is a reflection of the internal energy relationship but not a cause.

The heat loss in the pulse tube gets decreased by the DC flow, with its distributed sensible refrigeration power. The heat loss can be simplified to be proportional to the temperature gradient in the pulse tube, similar to that at the regenerator. When the pressure-induced enthalpy flow is negative, the temperature gradient becomes steep, and the loss is significant, as shown in Fig. 13. Previous experiments showed that the heat loss is reduced when the temperature gradient is decreased [77]. Previous simulation showed that the temperature profile at the cold part in the pulse tube gets closer to be flat as the DC flow gets larger, as shown in Fig. 29. This means that the temperature gradient in more part of the gas turns to be close to zero if more DC flow is exerted. In this case, the enthalpy flow of the AC flow gets closer to the PV power in the pulse tube, which means that the expansion efficiency of the pulse tube approaches 100%. A recent simulation on a Vuilleumier-type PTR showed that the enthalpy flow of the AC flow (noted as H_AC_PT) gets larger as the DC flow increases in the pulse tube, and the expansion efficiency also increases [78], as shown in Fig. 30.

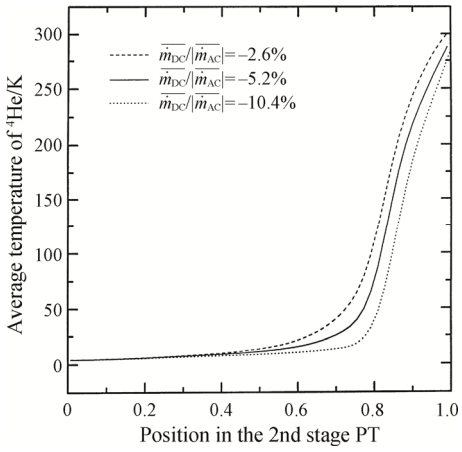

Fig. 29 Calculated temperature profiles along the pulse tube when it is superimposed with various amount of the DC flow [76]

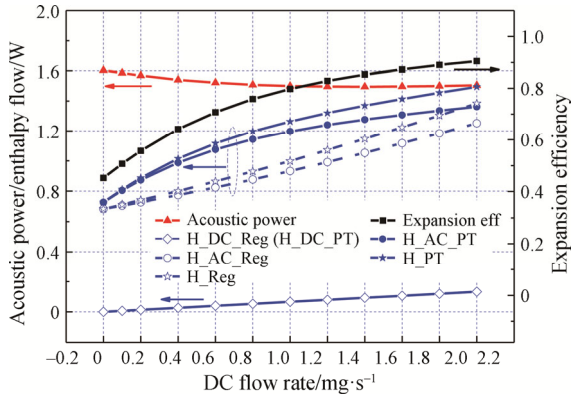

Fig. 30 Dependence of the enthalpy flows and the expansion efficiency on the DC flow in the pulse tube. The cold-end temperature is fixed at 15 K [78]

Here we propose an attenuation coefficient noted as ε_{PT}, which is defined as the increasing value of the enthalpy flow of the AC flow at the cold end divided by the distributed refrigeration power of the DC flow, shown as this equation:

$$\varepsilon_{PT} = \frac{\Delta\left\langle \dot{H} \right\rangle_{PT,c}}{\dot{m}_{DC}\int_{T_c}^{T_{PT,h}} c_p \mathrm{d}T} \tag{30}$$

A pulse tube [75] working in the temperature range between a certain point at 20 K to 40 K and 300 K is simulated with Sage [28]. It shows that the coefficient is about 0.4 when the cold-end temperature is equal to 20 K, and it decreases steadily as the DC flow increases, as shown in Fig. 31.

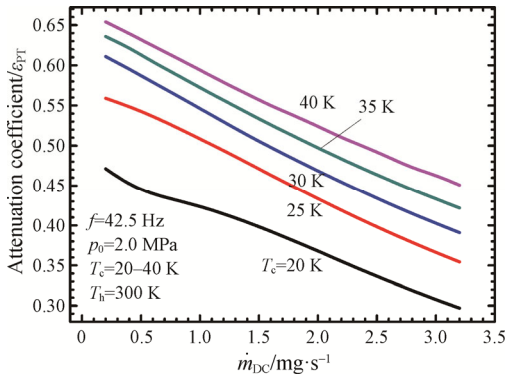

Fig. 31 Attenuation coefficient in the pulse tube (ε_{PT}) corresponding to various DC flow. The black, red, blue, cyan, and magenta lines represent a cold-end temperature of 20 K, 25 K, 30 K, 35 K, and 40 K, respectively.

What's more, an intermediate refrigeration power at the middle of the pulse tube was found to be significant [62]. It was measured to be as large as 0.75 W at 13.3 K in a case, comparable with the refrigeration power at the cold end (0.7 W at 3.58 K) [62]. It is reasonable to speculate that it was related to the distributed refrigeration power of the DC flow, where it was generated through the double-inlet valve. A sketch of the heat transfer process is shown in Fig. 32. It's only a speculation because there was no measurement of the DC flow or the internal energy flow.

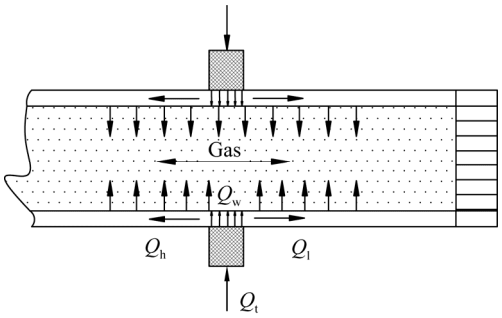

Fig. 32 Sketch of the heat transfer process of extracting intermediate refrigeration power on the pulse tube (Adopted from [62] with permission from Elsevier). The Q_t, Q_h, Q_l and Q_w refer to the heat flows of the intermediate point, the high part, the lower part, and the wall.

The theory of attenuation coefficient can also be applied to the regenerator [57]. The heat load that is brought about by the DC flow decreases the heat-associated enthalpy flow of the AC flow in an ideal regenerator without any effect on the cold-end refrigeration power, if the pressure-induced enthalpy flow at the cold end is the maximum in the whole range. This was observed in the experiments where an intermediate refrigeration power was applied on the regenerator [62, 63]. However, the heat-associated enthalpy flow of the AC flow at the cold end increases in the case that the DC flow gets larger than the minimum DC flow $\left(\dot{m}_{DC,min}\right)$ in an ideal regenerator, or in another case that it is a practical regenerator, so the refrigeration power decreases. Fortunately, not all the enthalpy flow of the DC flow becomes the heat load at the cold end because of the imperfectness of the regenerator [57, 79]. We propose an attenuation coefficient for the regenerator, defined as the increasing value of the enthalpy flow of the AC flow at the cold end divided by the distributed enthalpy flow of the DC flow, noted as ε_R, shown as:

$$\varepsilon_R = \frac{\Delta\left\langle \dot{H} \right\rangle_{R,c}}{\dot{m}_{DC}\int_{T_c}^{T_{R,h}} c_p \mathrm{d}T}. \tag{31}$$

Note that the hot-end temperature of that section regenerator $T_{R,h}$ is not necessarily the same as the hot-end temperature of the pulse tube $T_{PT,h}$.

The attenuation coefficient of a Stirling-type and

GM-type regenerators over a DC flow range is simulated [80] with the software REGEN3.3 [15], and it is drawn in Fig. 33. The attenuation coefficient of GM-type regenerators is as small as between 0.1% and 4% when the DC flow is smaller than the minimum DC flow and the cold-end temperature is not larger than 7 K, in which case the pressure-induced enthalpy flow at the cold end is the maximum all along the regenerator. This value of the attenuation factor is very close to the theoretical analysis of an ideal regenerator (which is equal to zero). The attenuation coefficient of Stirling-type regenerators at the same temperature range is much larger, and it increases gradually. Note that the attenuation coefficient of the GM-type regenerator also varies gradually when the cold-end temperature is equal to or larger than 8 K because the pressure-induced enthalpy flow at the cold end is not the maximum in the whole regenerator.

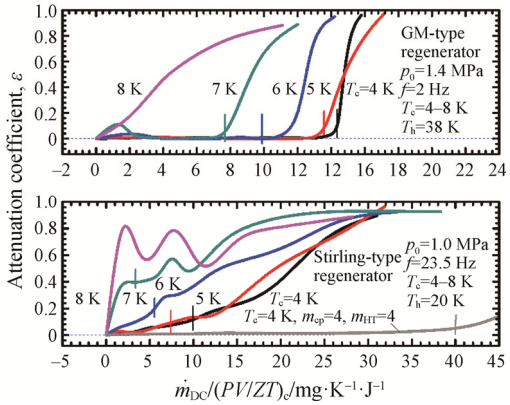

Fig. 33 Variation of the attenuation coefficient (ε_R) versus the characteristic DC flow for both the Stirling-type and GM-type regenerators [80]. The black, red, blue, cyan, and magenta lines represent a cold-end temperature of 4 K, 5 K, 6 K, 7 K, and 8 K, respectively.

The synthetic effect of the DC flow on the refrigeration power of the PTR is expressed as:

$$\begin{aligned}\Delta\dot{Q}_c &= \Delta\left\langle \dot{H}\right\rangle_{PT,c} - \Delta\left\langle \dot{H}\right\rangle_{R,c} \\ &= \varepsilon_{PT}\dot{m}_{DC}\int_{T_c}^{T_{PT,h}} c_p \mathrm{d}T - \varepsilon_R \dot{m}_{DC}\int_{T_c}^{T_{R,h}} c_p \mathrm{d}T\end{aligned} \tag{32}$$

Here some minor variations, including the heat conduction and the flow resistance that changes with the temperature profile, are omitted. It is clear that when the regenerator is heat-intercepted and the pulse tube works in a large temperature range, which is usually the case for 4 K GM-type PTRs [32, 39, 71, 76] and two-stage Stirling-type PTRs [60, 72, 75], the improvement of the refrigeration power with the DC flow is quite significant. Note that the heat load of the DC flow will certainly decrease the refrigeration power at upper stage(s) or increase the precooling load.

In some cases, the hot ends of the regenerator and the pulse tube are connected and isothermal (noted as T_h), especially for a single-stage PTR [76] or a 4 K Stirling-type PTR [40, 81], and the expression can be simplified as:

$$\Delta\dot{Q}_c = \left(\varepsilon_{PT} - \varepsilon_R\right)\dot{m}_{DC}\int_{T_c}^{T_h} c_p \mathrm{d}T \tag{33}$$

The improvement of the DC in this case is generally not remarkable. It was measured that the no-load temperature decreased by only 0.1 K to 0.2 K at the temperature of around 5 K [81, 82]. Another reason is that the attenuation coefficient ε_R of such regenerators is relatively large (around 0.2) because the regenerator efficiency of the Stirling type is relatively low, as shown in Fig. 33.

Several inferences are made based on this cognition of the attenuation effects on the pulse tube and the regenerator:

(1) The DC flow cannot improve the expansion efficiency of an ideal pulse tube. There is no heat transfer between the gas and the wall in such an ideal pulse tube, and the flow strengthening is perfect. So the expansion efficiency is 100% even though the real gas effects are serious. Any DC flow will cool down the gas in the pulse tube and result in a heat loss at the hot-end heat exchanger of the pulse tube.

(2) The DC flow generally improves the expansion efficiency in a practical pulse tube, no matter how serious the real gas effects are. The lower the original expansion efficiency of the pulse tube (the reasons include a small volume, a less efficiency of the flow strengthening and so on), the more improvement the DC flow will provide.

(3) The improvement with the DC flow is limited. The upper limit of the expansion efficiency of the pulse tube is 100%. Note that the decrease of the attenuation coefficient ε_{PT} as the DC flow increases is an indication. If a larger DC flow is exerted, the efficiency will not improve, but the temperature around the hot end will get lower, which generally means a waste of cold energy.

(4) There is an optimum point of improving the refrigeration performance with the DC flow method. The reason is that the two attenuation coefficients vary in contradictory trends. As the DC flow increases from zero, the attenuation coefficient of the regenerator increases from zero, while that of the pulse tube decreases from a relative large value, as shown in Fig. 31 and Fig. 33. The attenuation coefficient ε_R increases sharply after the minimum DC flow in a GM-type regenerator (shown in Fig. 33) and it soon surpasses the attenuation coefficient ε_{PT}, so the performance decreases at a speeding-up rate.

(5) It is possible to further improve the refrigeration efficiency if the DC flow induced from the regenerator gets divided into two portions: one portion is used for precooling the pulse tube, and the other portion is used

for providing intermediate refrigeration power for other applications. The precondition is that the regenerator is efficient and works close to or below the critical point, so the minimum DC flow is large and the attenuation coefficient ε_R is small. Meanwhile, the pulse tube is well designed and the required precooling power is small.

3.4 Decreasing losses in the clearance gap

It is almost a blank about the investigation on how to decrease the real gas losses in the clearance gap of the Stirling refrigerator or the GM refrigerator. Fortunately, the formation of the DC flow in these refrigerators has ever been theoretically explored [83], which demonstrated that the DC flow generally exists because of the density and velocity fluctuations in one cycle.

Here we carry out a preliminary simulation on a two-stage Stirling refrigerator that works down to 15 K [84]. An artificial mass flow pump is installed between the entrance to the second-stage regenerator and the hot end of the clearance gap, so that the DC flow in the loop can be controlled, as shown in Fig. 34.

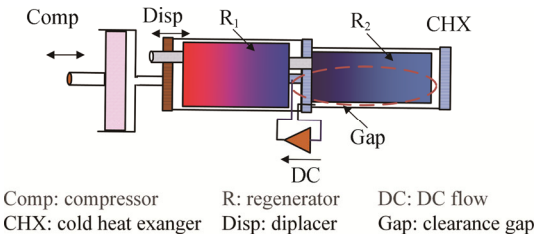

Fig. 34 Schematic of controlling the DC flow through the clearance gap in a two-stage Stirling refrigerator. An artificial mass flow pump is connected between the entrance to the second-stage regenerator and the hot end of the clearance gap. The red elliptical circle illustrates the possible DC flow in the loop.

It shows that the DC flow in the clearance gap is usually negative when there is no artificial mass flow pump, which means that the DC flow flows through the hot end of the clearance gap to the regenerator by way of the cold end. It is as large as –3.6 μg/s when the clearance is 10 μm. Most of the gas in the gap works at a high temperature in this case, as shown in Fig. 35. The negative DC flow generated in the original clearance gap carries a certain amount of enthalpy flow, which consumes the net refrigeration power, as shown in Fig. 36.

The artificial mass flow pump is able to generate a positive DC flow, and the temperature profile of the gas in the gap gets lower in this case. Meanwhile, losses in the clearance gas, including the shuttle heat loss and heat pumping loss, decrease significantly. In this case, the refrigeration power increases, as shown in Fig. 36. Similar to the PTR, comparison of the attenuation coefficients of the regenerator and the clearance gap (similar to that of the pulse tube) in the Stirling refrigerator is important to gain the refrigeration power, especially when the pressure-induced enthalpy flow is high. The difficulty is how to realize such a mass flow pump in practical refrigerators.

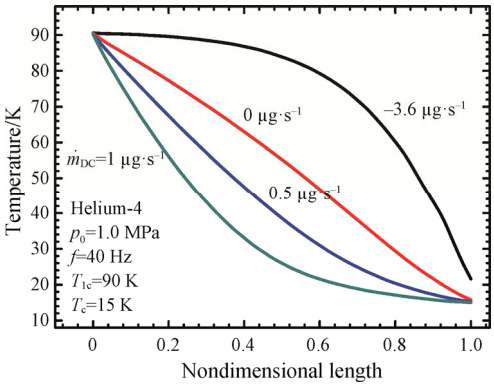

Fig. 35 Temperature profile of the gas in the clearance gap corresponding to various amount of the DC flow

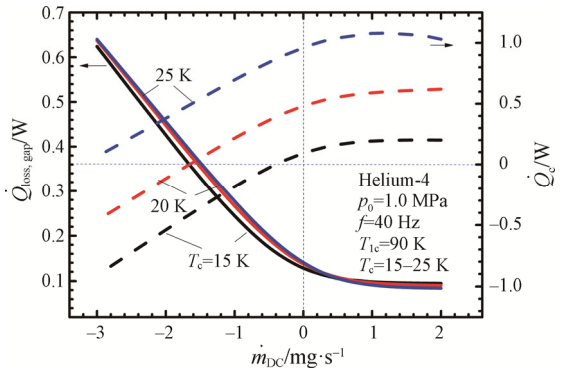

Fig. 36 Variation of heat losses in the clearance gap and the refrigeration power as the DC flow changes. The solid lines represent the heat losses, and the dash lines represent the refrigeration power. The black, red, and blue lines represent a cold-end temperature of 15 K, 20 K, and 25 K, respectively.

4. Discussion and Summary

We have reviewed the long history of exploring real gas effects which dates back to the 1970s. Important explorations in research areas including the loss terms in the regenerator, theoretical COP, ultimate refrigeration temperature, and effects on the pulse tube are summarized. The physical mechanism of reducing real gas losses, including the heat input or removal method and the DC flow method has been reviewed. We further explore some complicated phenomena related to real gas effects.

4.1 Main cognitions about real gas effects

It is emphasized in this paper that the main factor leading to the real gas losses in the regenerator is the heat-associated enthalpy flow, which is used to balance the variation of the pressure-induced enthalpy flow, resulting in an entropy generation. The real gas effects on the pulse tube is mainly the enlargement of the heat-associated enthalpy flow in the case when the pressure-induced enthalpy flow is negative, and thus the heat transfer between the gas and the wall gets enhanced.

A review of reducing the real gas losses has been carried out. The heat input or removal method is possible to eliminate all heat losses in the regenerator and to achieve a Carnot COP in the regenerator. The DC flow is a simplified and feasible method that decreases heat losses. The heat loss in the pulse tube or clearance gap gets decreased by the DC flow, and thus increases the expansion efficiency.

Here we would conclude that there are only the heat input or removal method and the DC flow method that can reduce the loss.

According to the first law of thermodynamics in an open oscillating system [7], it is only the terms of heat flow, enthalpy flow carried with a mass flow, and external work that are able to interact with the internal energy of the system. The equation is expressed as:

$$\left\langle \dot{Q} \right\rangle = \left\langle p\dot{V} \right\rangle + \dot{m}_{\mathrm{ex}} \left\langle \dot{h} \right\rangle_{\mathrm{ex}} - \dot{m}_{\mathrm{in}} \left\langle \dot{h} \right\rangle_{\mathrm{in}} + \frac{\mathrm{d}\left\langle U \right\rangle}{\mathrm{d}t} \quad (34)$$

The energy balance problem caused by real gas effects varies with temperature or location. The heat input or removal can be added at certain locations and the heat of DC flow is spreaded with a fixed distribution, which is able to fit that energy variation. However, the external work changes the pressure of the whole regenerator and adds to the PV power homogeneously all along the regenerator, because the pressure always spreads with the speed of sound, and it is not feasible. So the external heat flow, whether it is transferred or transformed, and the external mass flow, are two sole terms that can interact with the internal energy of the oscillating flow.

4.2 Further studies

Previous measurements on gross parameters such as the temperature profile and the refrigeration power have well supported the theories that have been reviewed or studied in this paper. However, a direct verification of the theories about real gas effects requires a direct measurement of the parameters in the oscillating flow, such as the dynamic temperature, pressure, mass flow in the oscillating flow. In this case, the pressure-induced enthalpy flow and the heat-associated enthalpy flow can be determined based on those dynamic parameters. It requires a fast response on measuring those instantaneous parameters and an integration of those data in one cycle. Actually it is challenging to get accurate data and to control the possible accumulated error.

Acknowledgement

This work is supported by National Natural Science Foundation of China (No. 51506152 and No. 51777141) and the Fundamental Research Funds for the Central Universities (inter-disciplinary program) under the contract No. kx0080020173427. The revision of this manuscript by Prof. D. Roundy (emeritus) from Tongji University, and now an adjunct professor with BYU Hawaii, is acknowledged.

References

[1] Zhang A.K., Wu Y.N., Liu S.S., Yu H.Q., Yang B.Y., Development of pulse tube cryocoolers at SITP for space application. Journal of Low Temperature Physics, 2018, 191: 228–241.

[2] Zhang A.K., Wu Y.N., Liu S.S., Zhu H.F., Zeng Y.P., Jiang Z.H., et al., Effect of impedance on a compressor driving pulse tube refrigerator. Applied Thermal Engineering, 2017, 124: 688–694.

[3] Radebaugh R., The state of the art and recent developments. Journal of Physics Condensed Matter, 2009, 21(16): 164–219.

[4] Zhu S.M., Yu G.Y., Li X.W., Ying M., Yan C.G., Dai W., et al., Acoustic field characteristics of a free-piston Stirling cryocooler with large cooling capacity at liquid nitrogen temperature. Applied Thermal Engineering, 2019, 147: 324–335.

[5] Nast T., Olson J., Champagne P., Evtimov B., Frank D., Roth E., et al., Overview of Lockheed Martin cryocoolers. Cryogenics, 2006, 46(2–3): 164–168.

[6] Walker G., Cryocoolers (Part 1: Fundamentals & Part 2: Applications). New York and London, 1983.

[7] Radebaugh R., Thermodynamics of regenerative refrigerators. Generation of Low Temperature and Its Applications, Shonan Tech. Center, Kamakura, Japan, 2003: 1–20.

[8] Wang K., Dubey S., Choo F.H., Duan F., Modelling of pulse tube refrigerators with inertance tube and mass-spring feedback mechanism. Applied Energy, 2016, 171: 172–183.

[9] Zen D., Ao Y., Zhang X., Liu C., Engineering thermodynamics, third ed., Beijing, 2002. (in Chinese)

[10] Lemmon E.W., McLinden M., Huber M., NIST Standard Reference Database 23, NIST Reference Fluid Thermodynamic and Transport Properties-REFPROP, 2002.

[11] Huang Y.H., Chen G.B., Arp V.D., Debye equation of

state for fluid helium-3. The Journal of Chemical Physics, 2006, 125(5): 1–10.

[12] Putintsev N.M., Putintsev D.N., Heat capacity and thermal expansion of water and helium. Journal of Thermal Science, 2017, 26(2): 125–131.

[13] Radebaugh R., Huang Y., O'Gallagher A., Gary J., Calculated regenerator performance at 4 K with helium-4 and helium-3. Advances in Cryogenic Engineering 53, Chattanooga, TN, Melville, 2008, 985(1): 225–234.

[14] Cao Q., Qiu L.M., Gan Z.H., Real gas effects on the temperature profile of regenerators. Cryogenics, 2014, 61: 31–37.

[15] Gary J., O'Gallagher A., Radebaugh R., Huang Y., Marquardt E., REGEN3.3: User Manual. 2006.

[16] Schmidt G., The theory of Lehmann's calorimetric machine. Z Ver Dtsch Ing 1871.

[17] Finkelstein T., Thermodynamic analysis of stirling engines. Journal of Spacecraft and Rockets, 1967, 4(9): 1184–1189.

[18] Modest M.F., Tien C.L., Analysis of real-gas and matrix-conduction effects in cyclic cryogenic regenerators. Journal of Heat Transfer, 1973, 95(2): 199–205.

[19] Daney D.E., Cooling capacity of Stirling cryocoolers - the split cycle and nonideal gas effects. Cryogenics, 1982, 22(10): 531–535.

[20] Jin X., Ouyang R., Chen W., Effect of non-ideal gas on refrigerating capacity of G-M cryocooler. Journal of low-temperature physics, 1987, 9(2): 103–107.

[21] Wu P.Y., Research on the scheme of G-M cryocooler working at 4–5 K. Cryogenics and superconductivity, 1988, 2: 1–6. (in Chinese)

[22] Chen G., Sun G., Liang J., Effect of non-ideal working medium on performance of nonmetal cryogenic refrigerating machine. Journal of zhejiang university (natural science edition), 1989, 1: 141–149. (in Chinese)

[23] Jin X., Real gas effects in the VM refrigerator. Low Temperature and Specialty Gases, 1990, 2: 24–28. (in Chinese)

[24] Chen J., Yan Z., Effect of non-ideal heat recovery on performance of Stirling refrigerating machine. Cryogenic engineering, 1991, 6: 37–41. (in Chinese)

[25] Yan Z.J., Inherent non-ideal regenerative properties of Stirling refrigerating machines working with the neon. Low temperature and characteristic gases, 1993, 4: 28–31. (in Chinese)

[26] Barron R., Cryogenic systems, second ed., New York, 1985.

[27] Luo E.C., Dai W., Radebaugh R., Thermoacoustic and regenerative functions of alternating-flow regenerator. Journal of Engineering Thermophysics, 2006, 1: 1–4. (in Chinese)

[28] Gedeon D., Sage: Object-oriented software for cryocooler design. Proceedings of the 8th International Cryocooler Conference, New York, America, 1995, 8: 281–292.

[29] Wang C., Numerical analysis of 4 K pulse tube coolers: Part I. Numerical simulation. Cryogenics, 1997, 37(4): 207–213.

[30] Ju Y.L., De Waele A.T.A.M., A computational model for two-stage 4K-pulse tube cooler: Part I. theoretical model and numerical method. Journal of Thermal Science, 2002, 10(4): 342–347.

[31] Lang A., Hafner H.U., Heiden C., Systematic investigations of regenerators for 4.2 K-refrigerators. Advances in Cryogenic Engineering, 1998, 43: 1573–1580.

[32] Chen G.B., Qiu L.M., Zheng J.Y., Yan P.D., Gan Z.H., Bai X., et al., Experimental study on a double-orifice two-stage pulse tube refrigerator. Cryogenics, 1997, 37(5): 271–273.

[33] Gao J.L., Matsubara Y., Experimental investigation of 4 K pulse tube refrigerator. Cryogenics, 1994, 34(1): 25–30.

[34] Kuriyama T., Ohtani Y., Nakagome H., et al., Temperature profile and mass flow rate distributions in regenerator of Gifford-McMahon refrigerator using magnetic regenerator materials. Journal of Cryogenics and Superconductivity Society of Japan, 1996, 31(04): 203–208.

[35] De Waele A.T.A.M., Xu M.Y., Ju Y.L., Nonideal-gas effect in regenerators. Cryogenics, 1999, 39(10): 847–851.

[36] Kittel P., Enthalpy, entropy, and exergy flows real gas effects in ideal pulse tube cryocoolers. Advances in Cryogenic Engineering, 2006, 51: 345–352.

[37] Wang C., Numerical analysis of 4 K pulse tube coolers: Part II. Performances and internal processes. Cryogenics, 1997, 37(4): 215–220.

[38] Gao J.L., Hiresaki Y., Matsubara Y., A hybrid two-stage refrigerator operated at temperatures below 4K. Advances in Cryogenic Engineering, 1996, 41: 1495–1502.

[39] Xu M.Y., de Waele A., Ju Y.L., A pulse tube refrigerator below 2 K. Cryogenics, 1999, 39(10): 865–869.

[40] Cao Q., Qiu L.M., Zhi X.Q., Han L., Gan Z.H., Zhang X.B., et al., Impedance magnitude optimization of the regenerator in Stirling pulse tube cryocoolers working at liquid-helium temperatures. Cryogenics, 2013, 58: 38–44.

[41] Will M.E., De Waele A.T.A.M., Ideal pulse-tube refrigerators with real gases. Journal of Applied Physics, 2005, 98(4): 1–4.

[42] Cao Q., Real gas effects on the COP of regenerators working at low temperatures. Proceedings of the 19th International Cryocooler Conference, Boulder, America, 2016, 16: 319–323.

[43] Gan Z.H., Li Z.P., Chen J., Dai L., Qiu L.M., Design and preliminary experimental investigation of a 4 K

Stirling-type pulse tube cryocooler with precooling. Journal of Zhejiang University: Science A, 2009, 10(9): 1277–1284.

[44] Qiu L.M., Cao Q., Zhi X.Q., Han L., Gan Z.H., Yu Y.B., et al., Operating characteristics of a three-stage Stirling pulse tube cryocooler operating around 5 K. Cryogenics, 2012, 52(7–9): 382–388.

[45] Cao Q., Sun Z., Li Z.M., Luan M.K., Tang X., Li P., et al., Reduction of real gas losses with a DC flow in the regenerator of the refrigeration cycle. Applied Energy, 2019, 235: 139–146.

[46] De Waele A.T.A.M., Pulse-tube refrigerators: principle, recent developments, and prospects. Physica B: Condensed Matter, 2000, 280(1–4): 479–482.

[47] Kittel P., Ultimate temperature of pulse tube cryocoolers. Advances in Cryogenic Engineering, 2010, 55: 1601–1608.

[48] Thummes G., Bender S., Heiden C., Approaching the He-4 lambda line with a liquid nitrogen precooled two-stage pulse tube refrigerator. Cryogenics, 1996, 36(9): 709–711.

[49] Chen G.M., Chen G.B., Yu J.P., Study of the minimum refrigeration temperature of regenerative cryocoolers. Cryogenics, 1997, 37(7): 397–400.

[50] Jiang N., Lindemann U., Giebeler F., Thummes G., A 3He pulse tube cooler operating down to 1.3 K. Cryogenics, 2004, 44(11): 809–816.

[51] Nast T., Olson J., Roth E., Evtimov B., Frank D., Champagne P., Development of remote cooling systems for low-temperature, Space-Borne systems. Proceedings of the 14th International Cryocooler Conference, New York, America, 2007: 33–40.

[52] Qiu L.M., Han L., Zhi X.Q., Dietrich M., Gan Z.H., Thummes G., Investigation on phase shifting for a 4 K Stirling pulse tube cryocooler with He-3 as working fluid. Cryogenics, 2015, 69: 44–49.

[53] Chen L.B., Wu X.L., Liu X.M., Wang J., Xi X.T., Zhou Y., et al., Study on high-frequency pulse tube cryocoolers working in liquid-helium temperature range. Journal of Engineering Thermophysics, 2020, 41(5): 1073–1076.

[54] Nast T., Olson J., Champagne P., Mix J., Evtimov B., Roth E., et al., Development of a 4.5 K pulse tube cryocooler for superconducting electronics. Advances in Cryogenic Engineering, 2008, 53: 881–886.

[55] Watanabe A., Swift G.W., Brisson J.G., Measurements with a recuperative superfluid Stirling refrigerator. Advances in Cryogenic Engineering, 1996, 41: 1527–1533.

[56] Jahromi A.E., Miller F.K., A sub-Kelvin superfluid pulse tube refrigerator driven by paramagnetic fountain effect pump. Cryogenics, 2014, 62: 202–205.

[57] Radebaugh R., Regenerator behavior with heat input or removal at intermediate temperatures. Proceedings of the 11th International Cryocooler Conference, New York, America, 2001, pp. 409–418.

[58] Rawlins W., Radebaugh R., Bradley P.E., Timmerhaus K.D., Energy flows in an orifice pulse tube refrigerator. Advances in Cryogenic Engineering, 1994, 39: 1449–1456.

[59] Jung J., Jeong S., Expansion efficiency of pulse tube in pulse tube refrigerator including shuttle heat transfer effect. Cryogenics, 2005, 45(5): 386–396.

[60] Huang C., Cao Q., Zhi X., Xia X., Qiu L., Effects of DC flow on pulse tube cryocooler working at liquid hydrogen and liquid nitrogen temperatures. Applied Thermal Engineering, 2018, 137: 451–460.

[61] Ju Y.L., Real gas features on the performance of pulse tube cryocoolers. Advances in Cryogenic Engineering, 2002, 47: 950–957.

[62] Wang C., Intermediate cooling from pulse tube and regenerator in a 4 K pulse tube cryocooler. Cryogenics, 2008, 48(3–4): 154–159.

[63] Ravex A., Trollier T., Tanchon J., Prouve T., Free third-stage cooling for two-stage 4 K pulse tube cryocooler. Proceedings of the 14th International Cryocooler Conference, New York, America, 2007: 157–162.

[64] Zhu S.W., Ichikawa M., Nogawa M., Inoue T., 4K pulse tube refrigerator and excess cooling power. Advances in Cryogenic Engineering, 2002, 47: 633–640.

[65] Cao Q., Attainability of the Carnot efficiency with real gases in the regenerator of the refrigeration cycle. Applied Energy, 2018, 220(15): 705–712.

[66] Cao Q., Li Z., Luan M., Sun Z., Tang X., Li P., et al., Investigation on precooling effects of 4 K Stirling-type pulse tube cryocoolers. Journal of Thermal Science, 2019, 28(4): 714–726.

[67] Wang C., Thummes G., Heiden C., Experimental study of staging method for two-stage pulse tube refrigerators for liquid 4He temperatures. Cryogenics, 1997, 37(12): 857–863.

[68] Wang C., Helium liquefaction with a 4 K pulse tube cryocooler. Cryogenics, 2001, 41(7): 491–496.

[69] Choudhury A., Sahu S., Experimental helium liquefier with a GM cryocooler. Review of Scientific Instruments, 2017, 88(6): 1–6.

[70] Zhu S.W., Wu P.Y., Chen Z.Q., Double inlet pulse tube refrigerators: an important improvement. Cryogenics, 1990, 30(6): 514–520.

[71] Tsuchiya A., Xu M.Y., Investigation of DC flow effects on a 4K two-stage pulse tube cryocooler. 11th European Conference on Applied Superconductivity, Genoa, Italy, 2014: 1–4.

[72] Duval J.M., Charles I., Gauthier A., Trollier T., Tanchon J., Linder M., et al., Experimental results of 20 K pulse tube cold fingers for space applications. Proceedings of

the 15th International Cryocooler Conference, Long Beach, America, 2009, pp. 71–77.

[73] Ju Y., Wang C., Zhou Y., Dynamic experimental study of a multi-bypass pulse tube refrigerator with two-bypass tubes. Journal of Thermal Science, 1998, 7(1): 61–66.

[74] Hofmann A., DC flow in pulse tube coolers. Advances in Cryogenic Engineering, 2002, 47: 911–917.

[75] Cao Q., Investigation on refrigeration mechanism of multi-stage Stirling pulse tube cryocoolers working at liquid helium temperatures. Zhejiang University, Hangzhou, China, 2012.

[76] Wang C., Thummes G., Heiden C., Effects of DC gas flow on performance of two-stage 4 K pulse tube coolers. Cryogenics, 1998, 38(6): 689–695.

[77] Qiu L.M., Zhi X.Q., Han L., Cao Q., Gan Z.H., Performance improvement of multi-stage pulse tube cryocoolers with a self-precooled pulse tube. Cryogenics, 2012, 52(10): 575–579.

[78] Wang Y.N., Cui Y.H., Dai W., Pfotenhauer J.M., Wang X.T., Luo E.C., Effects of DC flow on a cryogen-free Vuilleumier type pulse tube cryocooler. International Journal of Refrigeration, 2020, 114: 148–154.

[79] Tang K., Feng Y., Jin T., Jin S., Yang R., Impact of Gedeon streaming on the efficiency of a double-inlet pulse tube refrigerator. Applied Thermal Engineering, 2017, 111: 445–454.

[80] Cao Q., Luan M.K., Huo B., Li Z.M., Sun Z., Li P., et al., Reduction of real gas losses with a DC flow in the practical regenerator of the refrigeration cycle. Applied Thermal Engineering, 2021, 183: 116123.

[81] Pan C.Z., Zhang T., Zhou Y., Wang J.J., A novel coupled VM-PT cryocooler operating at liquid helium temperature. Cryogenics, 2016, 77: 20–24.

[82] Han L., Qiu L.M., Gan Z.H., huang C., Xia X., Zhi X.Q., Effect of DC flow on a Stirling-type pulse tube cryocooler working around liquid-helium temperature range. Cryogenics, 2016, 5: 1–4. (in Chinese)

[83] Gedeon D., DC gas flows in stirling and pulse tube cryocoolers. In: Ross RG, editor. Proceedings of the 9th International Cryocooler Conference, New York, America, 1997: 385–392.

[84] Liu D., Li A., Li S., Wu Y., Performance of the SITP 35K two-stage Stirling cryocooler. Infrared Technology and Applications XXXVI, Orlando, America, 2010, 1–6.